Calibration of radar differential reflectivity using quasi-vertical profiles

Daniel Sanchez-Rivas and Miguel A Rico-Ramirez

Department of Civil Engineering, University of Bristol, Bristol, BS8 1TR, United Kingdom

Correspondence: Daniel Sanchez-Rivas (d.sanchezrivas@bristol.ac.uk)

Abstract. Accurate precipitation estimation with weather radars is essential for hydrological and meteorological applications. The differential reflectivity (Z_{DR}) is a crucial weather radar measurement that helps to improve quantitative precipitation estimates using polarimetric weather radars. However, a system bias between the horizontal and vertical channels generated by the radar produces an offset in Z_{DR}. Existing methods to calibrate Z_{DR} measurements rely on ~~vertical observations~~ the intrinsic values of Z_{DR} ~~taken in rain,~~ of natural targets (e.g., drizzle or dry snow) collected at high elevation angles (e.g., higher than 40° or even at 90°), in which Z_{DR} values close to 0 dB are expected. However, not all weather radar systems ~~are capable of producing vertical pointing measurements .~~ can scan at such high elevation angles or point the antenna vertically to collect precipitation measurements passing overhead. Therefore, there is a need to develop new methods to calibrate Z_{DR} measurements using lower elevation scans. In this work, we present and analyse a novel method for correcting and monitoring the Z_{DR} offset using quasi-vertical profiles ~~of polarimetric variables~~computed from scans collected at 9°elevations. The method is applied to radar data collected through one year of precipitation events by two operational C-band polarimetric weather radars in the UK. The proposed method ~~proves effective in achieving the required accuracy~~ shows a relative error of 0.1 dB ~~for the calibration of~~ when evaluated against the traditional approach based on Z_{DR} ~~as the calibration results are consistent with the traditional method based on vertical profiles~~measurements collected at 90°elevations. Additionally, the method is independently ~~evaluated~~ assessed using disdrometers located near the radar sites. The results showed a ~~good~~ reasonable agreement between disdrometer-derived and radar-calibrated Z_{DR} measurements.

1 Introduction

~~The differential reflectivity~~ Conventional weather radars transmit signals in the microwave frequency range that are backscattered towards the radar antenna when precipitation particles (also known as hydrometeors, including raindrops, snow, melting snow, hail, graupel) lie along the path of the radar beam. The signal backscattered by hydrometeors is related to the radar reflectivity Z that can be converted to an estimation of rainfall rate R using a power-law equation $Z = aR^b$. Dual-polarisation weather radars measure the radar reflectivity at horizontal Z_H and vertical Z_V polarisations, and the ratio between both of them is known as the differential reflectivity Z_{DR}. Z_{DR} was proposed to improve radar rainfall estimation because raindrops are distorted into oblate spheroids as they fall to the ground (Pruppacher and Beard, 1970; Seliga and Bringi, 1976). Small raindrops give Z_{DR} values close to zero, whereas larger raindrops give $Z_{DR} > 0$. The differential reflectivity (Z_{DR}) plays a ~~key~~ crucial role in

quantitative precipitation estimation (QPE) algorithms using polarimetric weather radars. Its relation with the orientation, shape and size of the hydrometeors improves not only the accuracy of radar QPE algorithms ~~and hydrometeor classification systems (Al-Sakka et al., 2013; Bringi et al., 2011; Chandrasekar and Bringi, 1988; Cifelli et al., 2011; Giangrande and Ryzhkov, 2008; Gou et al.~~ (Bringi et al., 2011; Cifelli et al., 2011; Giangrande and Ryzhkov, 2008; Ryzhkov et al., 2005b; Vulpiani et al., 2009) but also the classification of hydrometeors (Al-Sakka et al., 2013; Besic et al., 2016; Park et al., 2009; Straka et al., 2000).

~~But~~ However, to incorporate Z_{DR} as a valid input for radar QPE, it is necessary to ensure that it is properly calibrated. Ryzhkov et al. (2005a) showed that an accuracy of 0.2 dB in the differential reflectivity calibration is desirable for practical applications of polarimetric weather radar data, as this ~~figure~~ value generates uncertainty in the rain estimates close to 18%. However, several factors introduce a bias in Z_{DR}, e.g. (a) the presence of cross-polar radiation (Zrnić et al., 2010); (b) errors in the transmitter~~and/or receiver chain~~, and the receiver chain (or both) (Zrnic et al., 2006) or (c) an overall system bias due to the ratio of power transmitted to the horizontal and vertical polarisations (Bringi and Chandrasekar, 2001).

~~To~~ Several calibration procedures have been proposed to correct the overall system bias (or offset) in Z_{DR} ~~, several calibration procedures have been proposed~~ depending on the radar scanning strategy. For radars capable of performing measurements at 90° elevation angle (herein referred to as birdbath scans), the most accepted calibration procedure is based on ~~the observation of raindrops measured in light rain as the radar~~ radar observations of raindrops as the antenna rotates about the vertical; non-zero values of Z_{DR} present under these conditions can be set as the Z_{DR} offset. This method was introduced by Gorgucci et al. (1999) and has been further explored and validated on several radar campaigns, e.g., Bechini et al. (2002) used vertical profiles (VPs) generated from data collected by a weather radar located in Italy to estimate both the Z_{DR} offset and the error in the radar reflectivity (Z_H). They analysed the standard deviation of Z_{DR} taken at vertical incident and concluded that the accuracy of this method is close to 0.1 dB. Similarly, Gourley et al. (2009) estimated the Z_{DR} offset using birdbath scans collected by a C-band radar~~and demonstrates~~, and their results demonstrated its impact on the absolute calibration of Z_H; Louf et al. (2019) used polarimetric birdbath scans measured by a C-band radar located in Australia to validate a new approach for calibrating and monitoring Z_H using ground clutter and satellite data. Frech and Hubbert (2020) used data collected from the radar network operated by the German Meteorological Service to monitor the Z_{DR} calibration. Their method relies on range-averaged values of Z_{DR} collected in light rain and detected using thresholds on polarimetric variables like the co-polar correlation coefficient or the coherent power to target an accuracy on Z_{DR} of around ± 0.1 dB. More recently, Ferrone and Berne (2021) expanded the birdbath method by estimating the offset based on interpolated Z_{DR} values taken from rain, snow, or ice regions, being the main advantage of this method its applicability when rain regions are not available to estimate the Z_{DR} offset.

However, some weather radar networks are unable to perform birdbath scans due to mechanical constraints. So several procedures have been proposed to overcome this restriction and correct the Z_{DR} offset. Ryzhkov et al. (2005a) presented a method based on the Z_{DR} values of dry ~~aggregates~~ snow collected at elevation angles between 40° and 60°. They linked these values to the Z_{DR} offset, achieving an accuracy of 0.2 dB. Giangrande and Ryzhkov (2005) expanded this method for scans affected by the presence of partial beam blockage and explored its relation with the Z_{DR} offset, stating that this method achieves an accuracy of 0.3 dB when applied to large data sets. ~~It is worth noting that both methods require a pre-classification~~

~~of the hydrometeors before their implementation.~~ Bechini et al. (2008) proposed a method to quantify the Z_{DR} offset by probing the differential reflectivity while increasing the elevation ~~angles~~ angle but below the melting layer (ML). Then, this data is compared with theoretical profiles of Z_{DR} to estimate the Z_{DR} offset. Although it is possible to achieve high accuracy by applying this method (~ 0.1 dB), thousands of profiles are needed to generate profiles suitable for the comparison process.

Another well-known technique to calibrate Z_{DR} relies on sun measurements. It is based on the detection of solar spike echoes as this type of radiation has equal power at both horizontal and vertical polarisations (Gourley et al., 2006), hence generating measurements of Z_{DR} close to 0 dB. The sun-radiation detection method has been further investigated in several works, e.g. Gourley et al. (2006) compared both the birdbath scans and sun radiation detection methods using C-band polarimetric data, determining that higher accuracy is achieved when using the former. An ~~on-line~~ online variation of the solar-radiation detection method that does not require the operational scanning strategy to be stopped ~~,~~ was introduced by Holleman et al. (2010). It is based on other works conceived to monitor the absolute radar calibration, like the methods introduced by Darlington et al. (2003) and Huuskonen and Holleman (2007). This ~~on-line~~ online method enables monitoring the calibration of Z_{DR} and also the analysis of the correlation between horizontal and vertical ~~lobes~~channels. Later, Huuskonen et al. (2016) expanded this method based on data collected from the Finnish radar network, adding quality control to the solar signals and achieving accuracy on Z_{DR} below 0.05 dB. Chu et al. (2019) also used the sun radiation detection method and concluded that an accurate calibration depends on the availability of radar data taken at sunrise/sunset, among other considerations. It is worth noting that the offset detected by the solar method must be taken with care as it is related to the receiver chain only, whereas the offset computed from birdbath scans includes both the transmitter and the receiver chain (Huuskonen et al., 2016).

Some other alternative techniques have been proposed to complement the operational calibration and monitoring of Z_{DR}. Bringi et al. (2006) estimated the Z_{DR} offset ~~of~~ using Range-Height-Indicator (RHI) scans collected by a C-band polarimetric radar located in Japan~~by fitting intrinsic ice values of~~ . They probed Z_{DR} ~~to~~ in ice regions (i.e., at high altitudes) where values of 0 dB are expected and set the mean values of ~~a Gaussian distribution, whereas~~ the observed data as the Z_{DR} offset. Richardson et al. (2017) proposed the use of turbulent eddies to monitor the differential reflectivity as the nature of such scatters results in values of Z_{DR} close to 0 dB. Additionally, Ryzhkov et al. (2016) proposed the application of the quasi-vertical profiles (QVPs) approach to monitor the calibration of Z_{DR} using a similar rationale as in Ryzhkov et al. (2005a). This approach is explored by Griffin et al. (2020) or Kumjian et al. (2016), in which previously offset-corrected QVPs of Z_{DR} are used to describe processes like the ML and ice aggregation/riming. Although the QVPs are a ~~useful~~ valuable tool for monitoring the temporal evolution of precipitation and ~~certain~~ the microphysics of precipitation, there is little ~~to none amount of research using QVPS~~ research using QVPs in rain to estimate the Z_{DR} offset. Most of the Z_{DR} calibration methods described above (except for the method that relies on sun measurements) rely on higher elevation scans. There is a need to develop alternative methods that can be used when only lower elevation scans are available.

This study presents an operational method to correct the Z_{DR} offset that can be implemented using ~~quasi-vertical profiles~~ QVPs of polarimetric variables. The method is based on QVPs generated from ~~elevation angle scans of around 10~~scans with elevation angles of 9° and collected during light rain. These scans are usually available in operational radar scanning strategies deployed in radar networks worldwide, thus becoming ~~a great~~ an excellent option for radar networks not capable of collecting

measurements at vertical incidence. The C-band polarimetric weather radars developed by the UK Met Office (UKMO) can perform measurements at vertical incidence, allowing a thorough comparison of the performance of both methods. Additionally, we explore the temporal variation of the Z_{DR} offset using long-term observations collected by two operational weather radars. The calibrated Z_{DR} measurements are further compared with measurements from independent disdrometer observations located near the radar sites. The paper is organised as follows. In Section 2, we define the radar and disdrometer data sets used in this work. The two different methods used to calibrate the radar Z_{DR} are described in Section 3. In Section 4, we examine the performance of the proposed method using long-term data sets collected by two weather radars and several disdrometers. We discuss the methods and results in Section 5. Finally, we summarise the findings of this work in Section 6.

2 Data sets

2.1 Radar data sets

The raw polarimetric radar data sets were obtained from two C-band weather radars part of the UKMO operational weather radar network. The Chenies radar site is located at Hertfordshire, near London, United Kingdom (Met Office, 2013) and the Dean Hill radar site is located at Wiltshire, near Salisbury, United Kingdom (Met Office, 2021). Both radars transmit and receive signals at horizontal and vertical polarisations simultaneously, generating Plan-Position-Indicator (PPI) products ~~sampled using different length pulses~~ at various pulse lengths, revolutions per minute (RPM) and covering several elevation angles. The PPI products ~~containing~~ include measurements of reflectivity (Z_H), differential reflectivity (Z_{DR}), correlation coefficient (ρ_{HV}), differential propagation phase (Φ_{DP}) and radial velocity (V) ~~were~~ collected throughout 2018 to carry out a long-term analysis of the Z_{DR} calibration; such products and its processing are described next.

The birdbath scans are sampled ~~at vertical incidence with~~ with the radar antenna pointing vertically (i.e., 90°elevation angle) while at the same time the antenna rotates around its axis (from 0°to 360°in azimuth). The scans have a temporal resolution of 10 minutes, 75 metres of gate resolution and a maximum range ~~cover~~ (equivalent to height for vertical scans) of 12 kilometres. These products are used to build ~~VPs~~ vertical profiles (VPs) of polarimetric variables and monitor the Z_{DR} calibration. The VPs are generated by averaging ~~azimuthally~~ raw polarimetric data taken from ~~birdbath scans but avoiding the~~ 360 vertical rays following the procedure suggested by Bechini et al. (2002); however, the first kilometre in height is discarded to minimise the risk of ~~side-lobes~~ side-lobe contamination and the presence of other ~~artefacts~~ artifacts that could affect the Z_{DR} calibration. Also, the VPs are used as input for a ML detection algorithm to distinguish the precipitation in the liquid phase, as described in Sanchez-Rivas and Rico-Ramirez (2021). These VPs will be used to compute the true Z_{DR} calibration offset, which will be used to validate the proposed algorithm. Note that this Z_{DR} offset is not error-free but provides a reliable benchmark to validate our algorithm.

PPI scans at 9° elevation angle are collected every 10 minutes and sampled ~~on~~ in Short Pulse (SP) mode (pulse length equal to 500 μs), with a gate resolution of 600 metres and a maximum range of 115 kilometres. These scans are processed to generate QVPs of polarimetric variables following the procedure suggested by Ryzhkov et al. (2016), averaging azimuthally

the polarimetric variables and generating one QVP of each polarimetric variable per PPI scan. As above, these data are also used to detect the ML. ~~The QVPs will also~~ These QVPs will be used to calibrate and monitor Z_{DR} using lower elevation scans.

PPI scans at 0.5°, 1.0° and 2.0° elevation angles are collected every 5 minutes and sampled ~~on~~ in Long Pulse (LP) mode (pulse length equal to 2,000 μs), covering a range of 250 kilometres and the same gate-resolution as above. These low-elevation angles are used to compare ~~calibrated~~ the offset-corrected radar Z_{DR} with Z_{DR} values derived from disdrometer data. ~~To remove non-meteorological echoes, a~~ A fuzzy logic classifier is applied using the methodology proposed by Rico-Ramirez and Cluckie (2008) to remove non-meteorological echoes. Once the differential reflectivity has been calibrated, corrections for attenuation in Z_H and Z_{DR} are applied following the methods ~~presented~~ described by Rico-Ramirez (2012) and Bringi et al. (2001) respectively.

It is important that the UK Met Office continuously monitors the quality of the radar reflectivity (Harrison et al., 2012, 2017), hence no Z_H calibration process is required.

The location and other relevant technical details of the radars are provided in Figure 1 and in Tables 1 and 2.

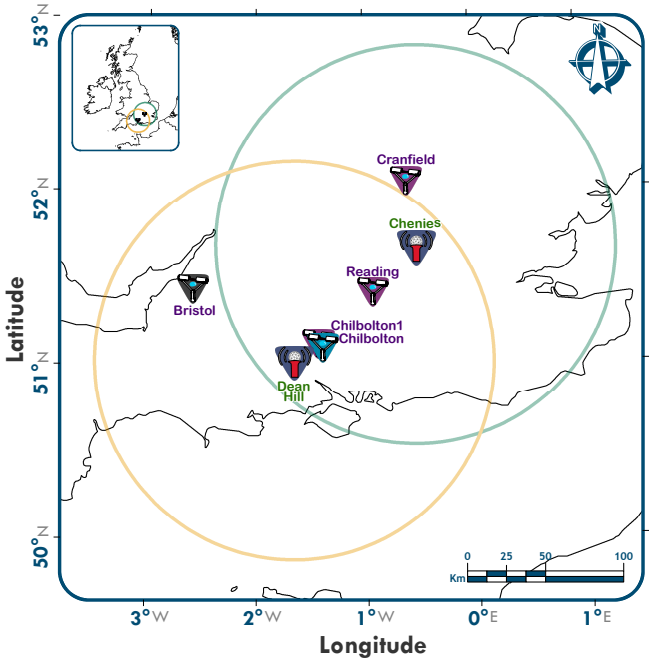

Figure 1. Location of the radars (Chenies and Dean Hill) and disdrometers (Bristol, Chilbolton, ~~Reading and~~ Cranfield and Reading). The circles represent the coverage of each radar at a distance of 115 km (maximum coverage of the radars operating at short pulse).

2.2 Disdrometer data sets

In this study, disdrometer data are used for verifying the consistency of the radar differential reflectivity measurements as the disdrometers are instruments that measure the drop size distribution (DSD) of precipitation. Several disdrometer data

Table 1. ~~Radars~~ Polarimetric radars characteristics.

Description	Wave length	Scanning strategy	Beam width	PRF	RPM
Chenies & Dean Hill C-band weather radars	5.3 cm	8 elevations (0.5°, 1°, 2°, 3°, 4°, 6°, 9° and 90°)	1.0°	900 *Hz* (SP) - 300 *Hz* (LP)	3.6 (SP) - 1.4 (LP)

Note: PRF=Pulse Repetition Frequency; RPM=Revolutions Per Minute; SP=Short Pulse; LP=Long Pulse.

sets were collected from different projects with neighbouring locations to the radar sites and matching time periods. These include disdrometers from the Chilbolton Facility for Atmospheric and Radio Research (CFARR), the Disdrometer Verification Network (DiVeN) and the University of Bristol (UoB) (see locations in Figure 1 and Table 2).

CFARR operates a Joss-Waldvogel impact disdrometer (model RD-69) located at Chilbolton, Hampshire, south England, providing continuous DSD data since 2003. The disdrometer converts the vertical momentum of a falling drop into signals whose amplitude depends on the diameter of the impacting drop. This device provides drop counts every 10 seconds over 127 bins ranging from 0.3 to 5 mm, with a sampling area of approximately 50 cm^2 (Science and Technology Facilities Council et al., 2003). This instrument does not measure the fall velocity of precipitation particles, and therefore the device does not provide a hydrometeor classification. For this work, data were available from January 2018 to July 2018.

DiVeN was deployed in 2017, ~~installing~~ and the disdrometer network includes several Thies laser precipitation monitors in the UK ~~and providing~~ that provide information on the quantity, intensity and type of precipitation (Pickering et al., 2019). The Thies ~~disdrometers classify the hydrometeors into one of~~ disdrometer measures the diameters and fall velocities of the hydrometeors and categorises hydrometeors into different classes (drizzle, drizzle/rain, rain, ice, snow, wet ice, wet snow, graupel, wet graupel and hail). The disdrometer provides the number of drops recorded every minute over a matrix covering 20 diameter ~~bins~~ and 22 velocity classes. The diameters range from 0.125 mm to 8 mm, ~~and one of the 22-speed bins~~ the velocities range from 0.0 ms^{-1} to 20.0 ms^{-1} ~~(Natural Environment Research Council et al., 2019). The~~ and the sampling area of ~~this~~ the instrument is approximately 45.6 cm^2 (Natural Environment Research Council et al., 2019). For this work, we selected three disdrometers operating near the radar sites, one at Chilbolton, Hampshire (herein Chilbolton1), one at Reading, Berkshire and one at Cranfield, Bedfordshire, all located in England. Data were collected for precipitation events throughout 2018.

The UoB operates several Parsivel2 disdrometers, one of them located at Bristol, southwest England. This ~~disdrometer~~ laser disdrometer measures the drop size distribution (DSD) and categorises the precipitation particles in several classes ~~, based on the volume equivalent diameter (~~(drizzle, drizzle/rain, rain, rain/snow, snow, sleet, hail). The instrument provides the number of drops recorded every minute over a matrix covering 32 diameter and 32 velocity classes. The particle size includes 32 bins ranging from ~~0~~ 0.2 to 25 mm ~~)~~ and the particle speed ~~(~~includes 32 bins ranging from 0.2 to 20 ms^{-1}) ~~, providing reliable~~

~~precipitation data including hydrometeor type and precipitation intensity~~ (OTT HydroMet, 2016). The sampling area of this instrument is approximately 50 cm^2. Data were collected for precipitation events throughout 2018.

Table 2. Summary of Radars (RAD) and disdrometers (DIS)~~locations and types~~.

Site Name	Facility	Model	D-CH	D-DH
Chenies	UKMO (RAD)	In-house design	-	107.18 km
Dean Hill	UKMO (RAD)	In-house design	107.18 km	-
Chilbolton	CFARR (DIS)	Joss-Waldvogel RD-69	87.40 km	19.79 km
Chilbolton1	DiVeN (DIS)	Thies	87.40 km	19.79 km
Cranfield	DiVeN (DIS)	Thies	43.28 km	136.28 km
Reading	DiVeN (DIS)	Thies	39.39 km	67.81km
Bristol	UoB (DIS)	Parsivel	143.66 km	76.19 km

Note: D-CH=Distance to the Chenies radar site; D-DH=Distance to the Dean Hill radar site.

2.2.1 Processing of disdrometer data.

The raindrop size distribution (DSD) can be computed from the disdrometer data by ~~Ji et al. (2019):~~ (Ji et al., 2019):

$$N_{mt}(D_i) = \frac{n_i(t)}{A.\Delta t.V_i.\Delta D_i} \frac{n_i(t)}{A \cdot \Delta t \cdot V_i \cdot \Delta D_i} \quad (1)$$

where D_i is the drop diameter in mm, n_i is the number of drops counted during the sampling interval Δt (s) at the ith bin size, A (m^2) is the sampling area of the disdrometer, V_i ($m\,s^{-1}$) is the terminal velocity of the raindrops at the ith bin size, ΔD_i (mm) is the ith bin width diameter interval. The sampling interval Δt was fixed to ~~1-min~~ 60s to ensure there is a sufficient number of measurements to compute a reliable DSD, which is also consistent with previous studies ~~(Bringi et al., 2011; Ji et al., 2019)~~ (Bringi et al., 2011; Ji et al., 2019). The terminal velocity of raindrops was computed by ~~Gunn and Kinzer (1949):~~ (Atlas et al., 1973):

$$V(D) = 9.65 - 10.3\exp(-0.6D_i) \quad (2)$$

where D is in mm and V is in m/s. The disdrometers measure the DSDs with a 1-min sampling interval. The Thies and Parsivel disdrometers measure the terminal velocity of raindrops ~~and so they can~~ to classify precipitation particles based on the velocity-diameter ~~relationship~~relationships. Only those measurements classified as liquid rain were used in this analysis. The DSDs were fitted to a normalised gamma drop size distribution using the procedure given in Bringi et al. (2003), where the normalised gamma DSD is given by:

$$N(D) = N_w f(\mu) \left(\frac{D}{D_m}\right)^{\mu} \exp\left[-(4+\mu)\frac{D}{D_m}\right] \quad (3)$$

where $f(\mu)$ is given by:

$$f(\mu) = \frac{6}{4^4}\frac{(\mu+4)^{\mu+4}}{\Gamma(\mu+4)} \tag{4}$$

where N_w (m^{3} $^{-3}$ mm^{-1}) represents the normalised intercept parameter, D_m (mm) is the mass-weighted mean diameter, and μ is the shape of the distribution. D_m is related to D_0 (median volume diameter) for a gamma DSD ~~with:~~ by (Bringi et al., 2003):

$$\frac{D_0}{D_m} = \frac{3.67+\mu}{4+\mu} \tag{5}$$

From the above analysis, the parameters N_w, D_0 (or D_m) and μ were retrieved for each 1-min measured DSD. Then, Eq. (3) was used to compute the theoretical DSD, which was used as input to a T-matrix scattering model developed by Mishchenko (2000) and adapted to compute all the different polarimetric weather radar measurements, including Z_H and Z_{DR}, which are both used in this analysis. The scattering simulations were performed using the following assumptions: (i) the raindrop shape model from Thurai et al. (2007) (their Eq. (2) for $D > 1.5$ mm, their Eq. (3) for $0.7 <= D <= 1.5$ mm, spherical raindrops otherwise); (ii) no canting angle distribution; (iii) maximum diameter for the integration fixed to $3D_0$; (iii) temperature of 10 °C, radar wavelength of 5.3 cm and elevation angle of 0 degrees.

3 Methods

3.1 Offset detection and monitoring of Z_{DR} using vertical profiles (VPs)

The overall system bias (or offset) in Z_{DR} can be estimated using VPs taken in light rain ~~as proposed by Gorgucci et al. (1999)~~ events, as described in the literature review. The VPs represent averaged observations of the 360 vertical rays, reducing the variance in Z_{DR} caused by the symmetry axis and the variety of shapes of the raindrops. Then, the premise of this method is to use VPs related to light rain, where a deviation from 0 dB in the rain region of the VPs can be set as the Z_{DR} offset. An in-depth discussion on the selection of this natural target to detect the Z_{DR} offset is provided in Section 5.

The offset on Z_{DR} can be detected and corrected by an automated operational procedure as follows:

1. It is necessary to detect the rain region on the VPs; this can be ~~done through a~~ achieved by implementing the ML detection algorithm ~~(e.g. see Sanchez-Rivas and Rico-Ramirez (2021))~~ proposed by Sanchez-Rivas and Rico-Ramirez (2021) and then setting the ML bottom as a boundary. Values on the VPs below ~~this height~~ the bottom of the ML are likely related to precipitation in the liquid phase.

2. Once the rain region is identified on the VPs, thresholds related to light rain are set, and only VPs containing two or more consecutive bins of Z_{DR} having corresponding values of 5 dBZ $< Z_H <$ 30 dBZ and $\rho_{HV} > 0.98$ are kept for further calculations.

3. The Z_{DR} offset is calculated for each VP related to light rain using the following expression:

$$Z_{DR}^{O_{VP}} = \frac{1}{n}\sum_{i=1}^{n} Z_{DR_i} \tag{6}$$

where i represents a valid bin along the VP, n the number of valid bins below the melting layer and avoiding clutter echoes, $Z_{DR}^{O_{VP}}$ is the offset calculated from the vertical profile and Z_{DR_i} represents the bins of Z_{DR} below the ML. Note that n includes bins from different azimuths. If $Z_{DR}^{O_{VP}}$ is different from 0 dB, then Z_{DR} needs to be calibrated.

4. Finally, Z_{DR} PPI measurements at different elevation angles can be corrected by subtracting the offset computed in Equation 6 to the original Z_{DR} measurements using:

$$Z_{DR}^{O_c} = Z_{DR}^{m} - Z_{DR}^{O_{VP}} \tag{7}$$

where $Z_{DR}^{O_c}$ is the offset-corrected differential reflectivity, Z_{DR}^{m} is the differential reflectivity measured by the radar and $Z_{DR}^{O_{VP}}$ is the offset calculated from the vertical profiles.

~~In Figure ??, the left panel shows VPs of Z_{DR} in a height-versus-time-plot related to a rain event recorded by the Chenies radar, whereas the right panel shows a single VP version taken from the same event. Figure ?? shows a persistent offset in Z_{DR} as the values of this variable in the rain medium are deviated from 0 dB below the bottom of the bright band (BB_{bottom}). The figure also shows that the first kilometre of the VPs is contaminated with spurious echoes, hence all bins below this height are discarded from the analysis. As shown in the right panel of Figure ??, the VP of Z_{DR} (representing the mean value of 360 rays) and its standard deviation (blue area) is steady in the rain region (below 1.5 km), but it turns noisy above the ML bottom (grey dotted line), showing a higher standard deviation. For this particular VP, the computed offset in Z_{DR} is -0.37 dB; this value is consistent throughout the whole event.~~

~~Collection of Z_{DR} VPs for a rain event recorded by the UKMO Chenies radar. The left panel displays VPs in a height-versus-time plot along with the melting level (MLe) and the bottom of the melting layer (BB_{bottom}). The right panel depicts a single VP and its standard deviation (std).~~

3.2 Offset detection and monitoring of Z_{DR} using ~~a~~ quasi-vertical profiles ~~approach~~(QVPs)

The QVPs of polarimetric variables provide insight into the evolution and structure of rain events through time, thus enabling monitoring the calibration of the radar variables. Hence, we propose a method to estimate the Z_{DR} offset that can be applied to QVPs generated from lower elevation scans with elevation angles of around ~~10~~9° ~~and~~ collected during light rain events. The ~~rationale supporting the~~ proposed method is ~~described as follows~~based on the following rationale:

a. The rain region within the QVPs of Z_{DR} is mostly uniform when the profiles are generated from data collected in light rain and near the radar as this region represents averaged observations of ~~oblate spheroid~~ small oblate raindrops. Figure 2 portrays the radar coverage of two PPI scans at different elevation angles recorded by one of the radars. It can be seen that birdbath scans (and subsequent VPs) capture uniformly the rain region (between 1 km and 2.5 km in height)

~~developing~~ developed above the radar (Figure 2(a)). Similarly, the rain region below the bright band (located at 2.5 km in height) is mostly homogeneous ~~when using a PPI from~~ for this particular PPI with an angle elevation of 9° (Figure 2(b)).

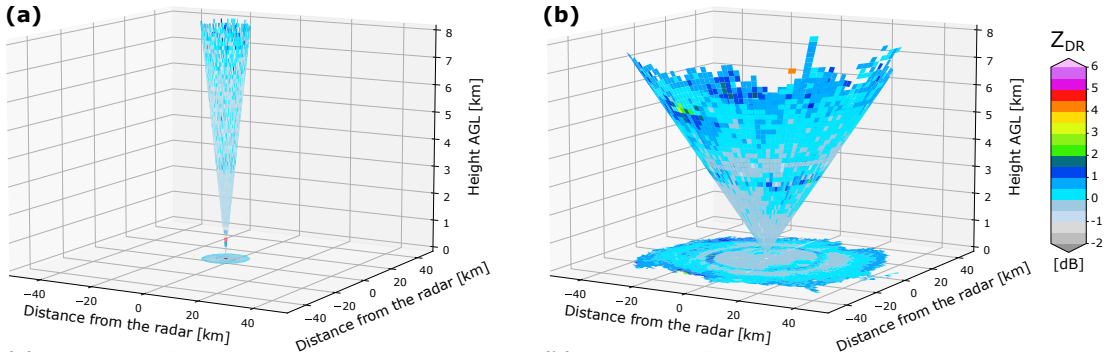

Figure 2. Representation of the radar conical coverage using (a) a birdbath scan, useful to build VPs and (b) a 9° PPI scan, used to generate QVPs.

b. The intrinsic value of Z_{DR} for angles below 90° and collected in light rain is ~~different from zero . Also,~~ larger than zero and it is elevation-dependent, as demonstrated by Bringi and Chandrasekar (2001) and formulated by Ryzhkov et al. (2005a) as:

$$Z_{dr}(\theta) \approx \frac{Z_{dr}(0)}{\left[Z_{dr}^{1/2}(0)\sin^2\theta + \cos^2\theta\right]^2} \tag{8}$$

where $Z_{dr}(0)$ and $Z_{dr}(\theta)$ represent the differential reflectivity in linear scale at elevation angles of 0° and θ°, respectively. Figure 3 displays the theoretical variation of Z_{DR} with elevation angle. It can be seen that the ~~variation of~~ difference in Z_{DR} ~~as a function of the the elevation can be neglected for elevations~~ values between an elevation below 10° ~~, in~~ and the elevation of 0° is negligible. In fact using Eq. (8) for $\theta = 10°$ results in Z_{dr} values very close to ~~one~~each other, that is:

$$Z_{dr}(\theta = 10°) \approx 0.968 Z_{dr}(\theta = 0°)\ \text{[dB]} \tag{9}$$

Hence, Z_{DR} radar measurements collected at elevation angles below 10° are similar to those collected at lower elevation angles and so they do not add additional uncertainty to the offset correction method. However, Figure 3 also shows that Z_{DR} values for lower elevation angles have a wide range of values (e.g. between 0 and 2 dB in this figure) compared with elevation angles of 90° in which Z_{DR} values close to zero are expected. This represents a challenge for our approach and therefore we have to constrain the Z_{dr} measurements used to compute the offset into a narrow band as explained next.

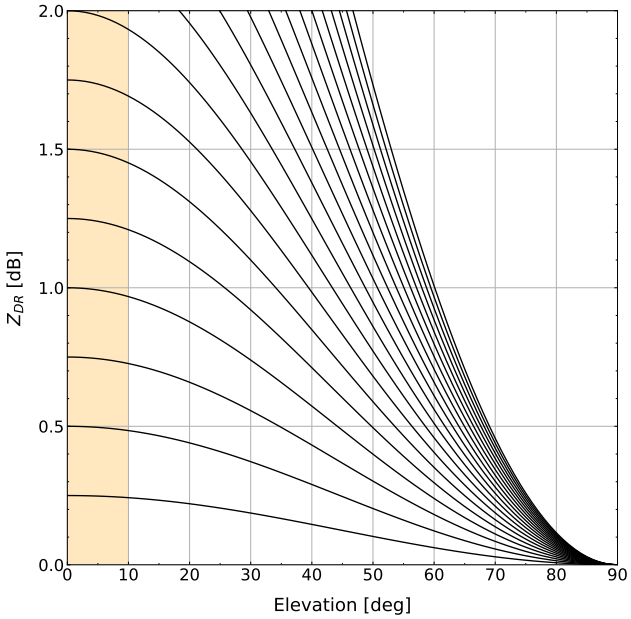

Figure 3. Theoretical dependencies of Z_{DR} at different elevation angles. Highlighted area shows the small variation of Z_{DR} for elevation angles below 10°.

c. We simulated a wide range of DSDs using the range of parameters described in Bringi and Chandrasekar (2001) expected in real storm events using the following parameter ranges:

$10^3 \leq N_w \leq 10^5$ $[mm^{-1}m^{-3}]$

$0.5 \leq D_0 \leq 2.5$ $[mm]$

$-1 \leq \mu \leq 5$

$R \leq 300$ $[mm\,h^{-1}]$

We randomly generated 10,000 sets of DSD parameters (Nw, D_0 and μ) uniform-distributed within the ranges defined above. Then, we use Equation 3 to simulate the DSDs, which are used as input to a T-matrix scattering model to compute Z_H and Z_{DR}. The scattering simulations are performed using the same assumptions described in section 2.2.1. The results of these simulation are shown in Figure 4(a), which depicts the theoretical variation of Z_{DR} versus Z_H, which is consistent with previous studies (Bechini et al., 2008; Bringi et al., 2006; Giangrande and Ryzhkov, 2005; Ryzhkov et al., 2005a) . Figure 4(a) shows that Z_{DR} increases with Z_H and also that Z_{DR} has a wide range of values for a given value of Z_H. However, the expected range of Z_{DR} measurements in light rain (e.g. for $Z_H < 20$ dBZ) becomes narrow and gives $Z_{DR} < 0.6$ dB (see zoomed region in Figure 4(a)).

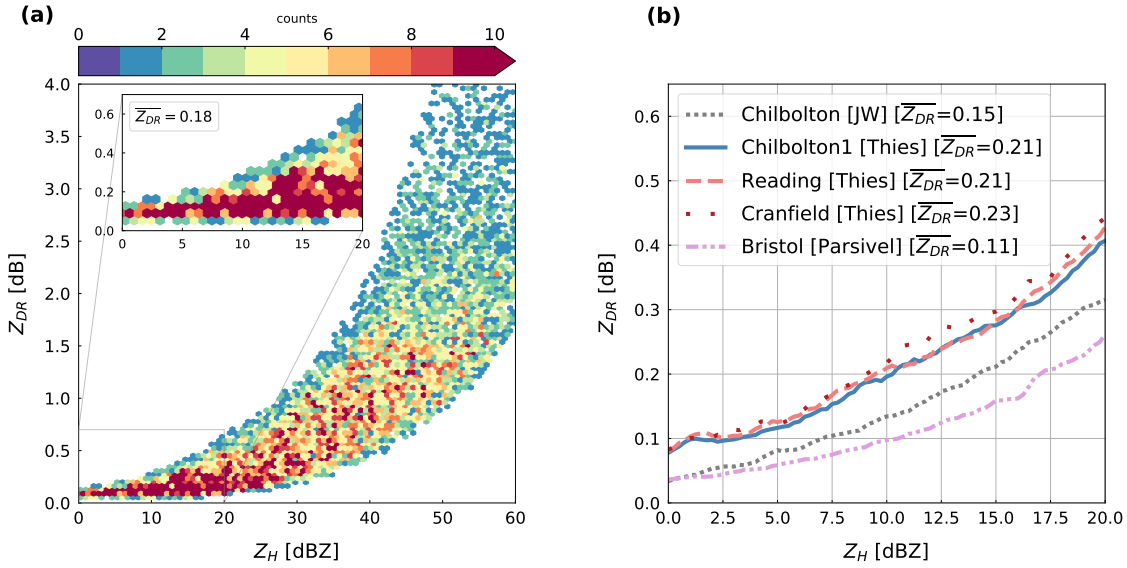

Figure 4. ~~Representation of the radar conical coverage using~~ (a) ~~a birdbath scan, useful to build VPs and~~ Simulated Z_H-Z_{DR} dependencies expected in real storm events; (b)~~a 9PPI scan, used to generate QVPs~~Z_H-Z_{DR} dependencies measured by several types of disdrometers at different loactions.

Based on the premises described above, we propose an operational method to ~~detect~~ compute and correct the Z_{DR} offset using QVPs ~~, and it is described next~~as described below.

1. As in the VPs method, the rain region is identified in the QVPs using a ML detection algorithm to set the ML bottom as a boundary. Values below this height are likely related to precipitation in the liquid phase. Additionally, a maximum height limit of 3 km is set to this ML bottom boundary to reduce the ~~effect of the varying diameter~~ range effects inherent to the generation process of the QVPs. The maximum height limit of 3km seems to work well in the UK, but it might need to be adjusted in other regions.

2. Using the ~~data sets described in section 2.2, we computed~~ theoretical variation of Z_H and Z_{DR} given in Figure 4(a) we compute the mean dependencies ~~of $Z_H - Z_{DR}$~~ but limited to a narrow range related to light rain (~~0-20~~ $0 < Z_H < 20$ dBZ), as shown in ~~Figure ??. Then, we compute the average value of these curves to include data from different disdrometer models and different locations into the analysis, thus setting 0.18 dB as the mean~~ the zoomed box in Figure 4(a). This yields a mean value of $\overline{Z_{DR}} = 0.18dB$, that it is set as the intrinsic value of Z_{DR} in light rain at ground level ~~.~~for lower elevation scans. This value is compared to $Z_H - Z_{DR}$ values computed from disdrometer measurements (see Figure 4(b)), confirming the good agreement between theoretical and measured Z_{DR} values.

3. ~~Thresholds~~ Various thresholds are set to detect QVPs related to light rain and discard bins within the QVPs related to mixed-phase precipitation. Thus, only QVPs containing ~~four~~ three or more consecutive bins of Z_{DR} with corresponding

values of 0 dBZ $< Z_H <$ 20 dBZ and $\rho_{HV} > 0.985$ on the QVPs of Z_H and ρ_{HV} respectively, are kept for further calculations. Note that the threshold set for Z_H is the same as the range selected in the ~~disdrometer data~~DSD simulations, whereas the threshold set for ρ_{HV} is more strict than in the method based on VPs ~~, this~~ in order to discard bins within the QVPs not related to light rain.

4. The average value of Z_{DR} is computed, calculating one value per QVP related to light rain:

$$Z_{DR}^{O_{QVP}} = \left(\frac{1}{n} \sum_{i=1}^{n} Z_{DR_i} \right) - 0.18 \text{ dB} \tag{10}$$

5. Finally, Z_{DR} measurements can be corrected by:

$$Z_{DR}^{Oc} = Z_{DR}^{m} - Z_{DR}^{O_{QVP}} \tag{11}$$

where Z_{DR}^{Oc} is the offset-corrected differential reflectivity, Z_{DR}^{m} is the differential reflectivity measured by the radar and $Z_{DR}^{O_{QVP}}$ is the offset calculated from the ~~quasi-vertical profiles~~QVPs.

~~Figure ?? shows~~

4 Long-term monitoring of the Z_{DR} calibration

We processed the radar data sets collected by two operational weather radars throughout one year of precipitation events to generate VPs and QVPs of polarimetric variables as described in Section 2.1. Then, we applied both Z_{DR} offset-correction methods to the generated VPs and QVPs to compare the results of the Z_{DR} calibration.

We present a rain event recorded in southern England by the Chenies radar to exemplify the abovementioned processes. In Figure 5(a), the left panel shows VPs (each one representing the mean value of 360 rays) of Z_{DR} in a height-versus-time (HTI) plot related to a rain event. In contrast, the right panel shows a single VP taken from the same event. Note that the first kilometre of the VPs is contaminated with spurious echoes; hence all bins below this height were discarded from the analysis. The HTI plot shows that the values of Z_{DR} deviate from 0 dB in the rain medium, i.e., below the bottom of the bright band (BB_{bottom}), thus Z_{DR} needs to be calibrated. The single VP plot enables an in-depth analysis of the profile characteristics. For example, it can be seen that Z_{DR} values within the rain region (below 1.5 km in height) are close to -0.35 dB and also that its standard deviation (std) remains relatively steady. But this changes in the ML, where the VP turns noisy and produces a higher standard deviation. However, dry aggregated snow signatures are visible above 2 km in height (at the top of the melting layer), where the Z_{DR} values are similar to those observed for liquid precipitation ($\sim$ 0.37 dB), confirming the reliability of dry snow to detect the Z_{DR} offset. These characteristics are consistent throughout the entire event.

On the other hand, Figure 5(b) shows QVPs of Z_{DR} generated from data ~~collected by a C-band weather radar~~related to the event described above. It can be seen that there are clear signatures of the melting layer ~~on~~ within the QVPs that are useful to classify the hydrometeors phase. ~~In the right panel of Figure ??, a QVP of Z_{DR} taken from the same event~~ The single QVP plot shows that the standard deviation of the averaged values used to generate the ~~profile is smaller on~~ QVP is smaller in the

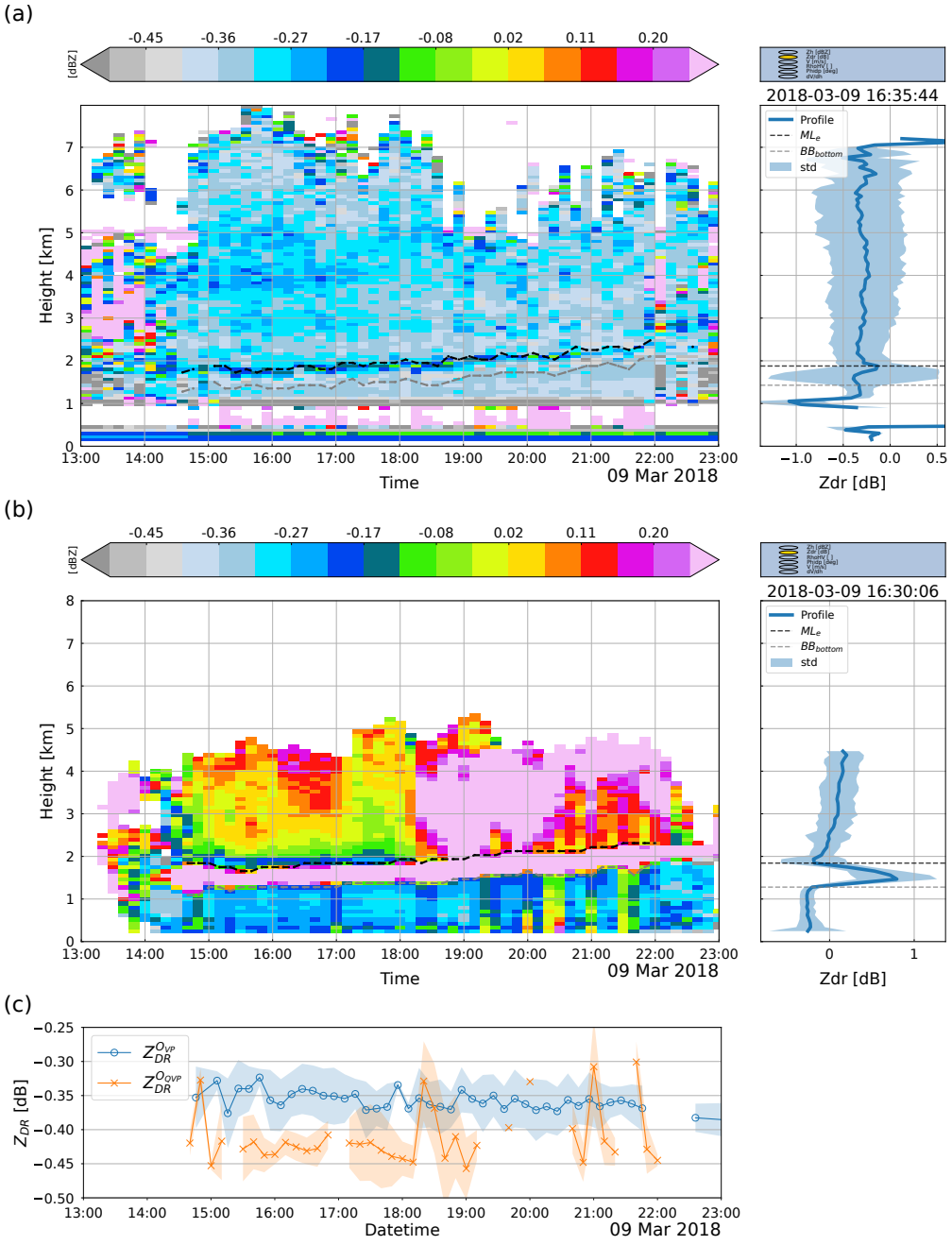

Figure 5. Rain event recorded by the UKMO Chenies radar on 09th May 2018. (a) shows a collection of Z_{DR} VPs in a height-versus-time plot along with the melting level (MLe) and the bottom of the melting layer (BB_{bottom}). Its right panel depicts a single VP and its standard deviation (std). (b) shows the same as in (a) but using QVPs of Z_{DR}. (c) shows the Z_{DR} offset computed using VPs (blue line, circle markers) and QVPs (orange line, cross markers); the filled areas represent the computed standard deviation for each data point.

rain region (below 1.35 km) compared to the standard deviation observed within and above the ML~~(above 1.3 km). For this example, the~~ . Moreover, the signatures of dry snow are not clearly visible, and the values observed for rain particles differ to those seen at the top of the ML, thus hampering using dry snow as the calibration target for our data sets. After applying the proposed method, the averaged value of Z_{DR} in the rain region is ~~-0.21~~ -0.26 dB that along with the computed intrinsic value of Z_{DR} (~~-0.18~~ 0.18 dB), results in an offset of ~~-0.39~~ -0.44 dB, which is ~~very~~ close to the offset calculated using the VPs method (~~-0.37~~ -0.35 dB).

~~Theoretical dependencies of Z_{DR} at different elevation angles. (a) Z_H-Z_{DR} dependencies simulated using Chilbolton disdrometer data set; (b) Mean Z_H-Z_{DR} dependencies simulated at several disdrometers locations. Collection of Z_{DR} QVPs for a rain event recorded by the UKMO Chenies radar. The left panel displays QVPs in a height-versus-time plot along with the melting level (MLe) and the bottom of the melting layer (BB_{bottom}). The right panel depicts a single QVP and its standard deviation.~~

5 ~~Long-term monitoring of the Z_{DR} calibration~~

~~The~~ Figure 5(c) shows the temporal variation of the Z_{DR} offset ~~is prone to fluctuate during short periods of time (daily or even hourly). These fluctuations can affect the rainfall estimations based on radar measurements; hence the~~ for both VPs (Z_{DR}^{OVP}) and QVPs (Z_{DR}^{OQVP}) methods. For this precipitation event, the differences between methods are around 0.1 dB. Still, it is worth mentioning that Z_{DR}^{OVP} exhibit values that remain relatively constant during this event, whereas the values of Z_{DR}^{OQVP} show greater variation, which is not altogether far from Z_{DR}^{OVP}. It is also important for this event that the number of valid VPs is larger than the number of QVPs classified as valid according to the proposed constraints described in the method. A discussion on the selection of the natural targets to detect the Z_{DR} ~~offset needs to be monitored, and Z_{DR} measurements need to be calibrated accordingly. We applied both Z_{DR} offset-correction methods on two radar data sets throughout one year of precipitation events to compare the results of the Z_{DR} calibration.~~ offset and the performance of the proposed method is provided in Section 5.

4.1 Validation of the QVPs-based approach using birdbath scans

The QVPs-based approach will be assessed by comparing its results with the ~~'true offset'~~ "true offset" computed from the VPs-based method since ~~this method~~ it is widely accepted and proven effective, as described in the literature review. Therefore, it is essential to highlight that the errors in the Z_{DR} calibration based on QVPs are relative to the traditional method. Additionally, both methods will be compared to independent measurements provided by the disdrometers.

4.2 ~~Validation of the QVPs-based approach using birdbath scans~~

~~We processed the radar data sets to generate VPs and QVPs of polarimetric variables for one year of radar data, as described in Section 2.1. Then, both the VPs-based and QVPs-based methods were applied to calibrate and monitor Z_{DR}.~~

Figure 6 shows the temporal variation of the Z_{DR} offset for the two ~~radars~~ radar datasets used in this work. For the Chenies radar data set (Figure 6(a)), it can be seen that the offset in Z_{DR} computed using the birdbath method fluctuates between -0.2 dB and -0.7 dB during most of the year. During February 2018, filters were installed at the Chenies radar, introducing a variation on the radar calibration that can be observed at this period (Timothy Darlington, Met Office, personal communication, 2021). The proposed method based on QVPs proves to be effective as the Z_{DR} offset values are similar to those calculated using VPs. For the Dean Hill radar data sets, the Z_{DR} offset varies ~~on a wider~~ in a broader range, but as above, the computed offset is similar on both methods. Similarly, an upgrade implemented on the Dean Hill radar during October 2018 modified the Z_{DR} calibration (Timothy Darlington, Met Office, personal communication, 2021), changing from -0.2 dB to 0.5 dB around this time of the year. ~~These results confirm the efficacy of the proposed method based on QVPs , achieving an accuracy of ± 0.1 dB compared to the method based on VPs~~However, a few points throughout the entire year exhibit more significant differences. This show that some profiles may surpass the constraints set to reject QVPs that do not meet the light rain criteria. Averaging the entire radar domain plays a key role here, as mixed-phase precipitation can affect the QVPs (see discussion in Section 5). Additionally, ~~the figure shows a particular rain event in a zoomed up window~~ Figure 6 shows two particular rain events (zoomed up boxes in this figure) for a deeper visualisation of the calibration methods~~. This figure shows~~ , where it can be seen that both methods produce similar results.

Figure 6 also shows that the number of profiles detected by each method is different. The VP-based method detects a larger number of profiles that meet the criteria of light rain, especially for the Dean Hill radar data set. For this radar data set, the number of valid profiles detected by the QVP-based approach represents 47% of the profiles detected by the VP-based method. This difference is not that big for the Chenies radar data set, as the number of profiles detected by the QVP-based method represents the 78% of profiles detected by the VP-based method. Although this is a limitation of the method, this ensures that only those QVPs due to light rain and with high ρ_{HV} values are used for the estimation of the Z_{DR} offset. In this case, we use the last valid QVP-based Z_{DR} offset, which is then compared to the Z_{DR} offset computed by the VP-based method.

Finally, we observed an overall relative error on the Z_{DR} offset using QVPs of ± 0.1 dB compared to the method based on VPs. This increase the confidence in using the proposed method based on QVPs.

~~Finally, we~~ We evaluate the outputs of each method for the two different radar sites using ~~different~~ metrics like the correlation coefficient (r), the mean absolute error (MAE), and the root mean squared error (RMSE). To effectively assess the performance of the ~~QVPs-based~~ QVP-based approach and its temporal variation, each computed offset value is ~~extended~~ stored as the radar Z_{DR} offset until a new ~~offset is computed~~one is detected, e.g., in Figure 6(ab), for the case on ~~09-March-2018~~24-May-2018, the VPs-based method yields a constant offset value of around ~~-0.36 dB between 19~~-0.15 dB between 13:05 and ~~20:45, whereas for the~~ 18:05, whereas he QVPs-based method ~~there are only three data points~~ only detected a handful of valid QVPs for the same ~~period of time , but~~ time period. However, the offset is similar at those points in time~~(-0.39 dB, -0.37 dBand -0.36 dB).~~ , with differences around ± 0.1 dB. It is worth mentioning that this is a warm rain event, and only a few QVPs meet the criteria set for detecting light rain.

Figure 7 shows ~~the~~ a comparison of the Z_{DR} offset estimated by both methods for both radars for the entire year. The results show that the Z_{DR} offset for the Chenies radar was between -0.7dB and -0.1 dB, with a small number of events showing

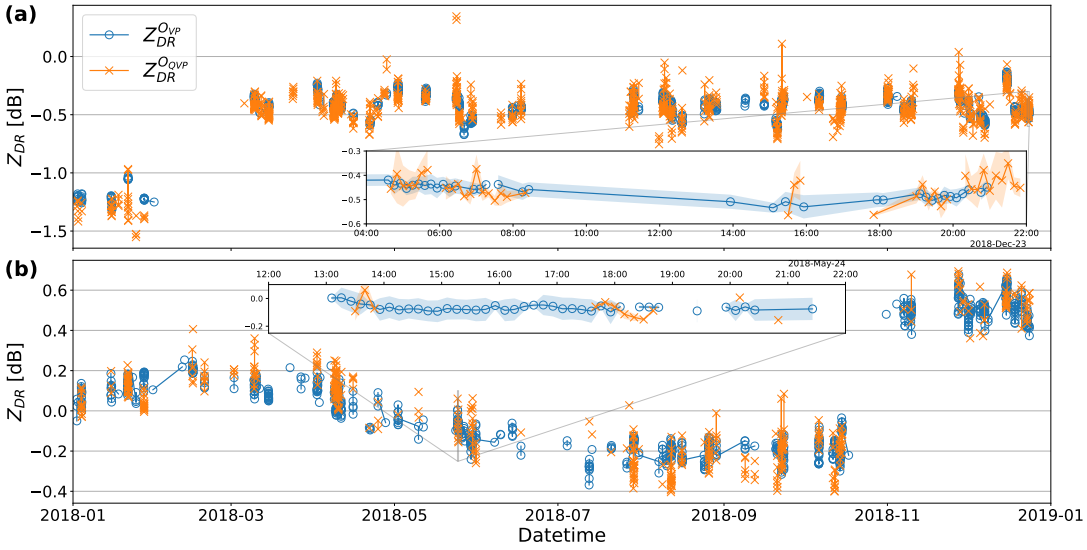

Figure 6. Temporal variation of the Z_{DR} offset on two weather radars during one year of rain events. The top panel shows the variation on the Chenies radar site, whilst the bottom panel depicts the offset variation at the Dean Hill radar site. The case of a rain event on 09 March 2018 is zoomed in on both panels for an in-depth examination.

an offset of around -1.3dB. For the Dean Hill radar, the Z_{DR} offset was between -0.4 dB and 0.6 dB. The figure shows a good correlation between the outputs of both methods, where ~~a global accuracy of the proposed method (±0.1 dB)~~ the relative performance of the QVP-based method is in good agreement ~~with the 'true offset'~~ (±0.1 dB) with the "true offset" computed from birdbath scans (VP-based method).

4.2 Differential reflectivity comparison using radar and disdrometers

Several validation procedures of the proposed method for correcting the Z_{DR} offset were performed utilising the disdrometer data sets described in Section 2.2. The fitted normalised gamma DSDs ~~allow~~ allows the estimation of the reflectivity and the differential reflectivity at ground level, enabling the validation of the QVPs-based method.

First, we compare the radar calibrated Z_{DR} measurements by the two approaches described in the previous sections at the disdrometer locations. Only individual radar bins exactly over the corresponding disdrometers locations are considered for comparison. Based on the distance between the radars and the disdrometers, we link the Cranfield and Reading disdrometers to the Chenies radar, whereas the Chilbolton1 disdrometer will be compared to the Dean Hill radar. ~~Note that the~~ The disdrometer located at Bristol was not used in this analysis because it is too far from both radar sites. In addition, we use the ~~classifiers~~ hydrometeor classification produced by the Thies disdrometers to evaluate ~~radar data only~~ the radar measurements related to liquid precipitation, as these disdrometers provide information about the rain type and intensity. This classification is helpful to discard DSDs related to snow or hail.

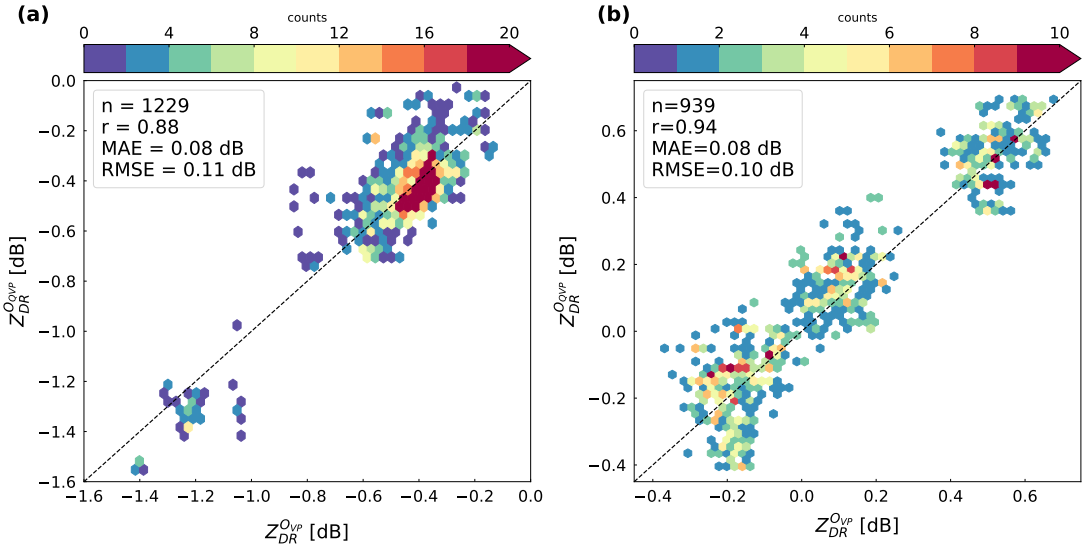

Figure 7. ~~Z_{DR} offset comparison on two radar data sets~~ Comparison of ~~the QVPs-based method versus the method based on birdbath scans~~ Z_{DR} offsets computed with QVPs and VPs. The scatter density plot shown in (a) provides metrics for evaluating the methods applied to the Chenies radar data set; whereas (b) shows the same as in (a) but for the Dean Hill radar data set.

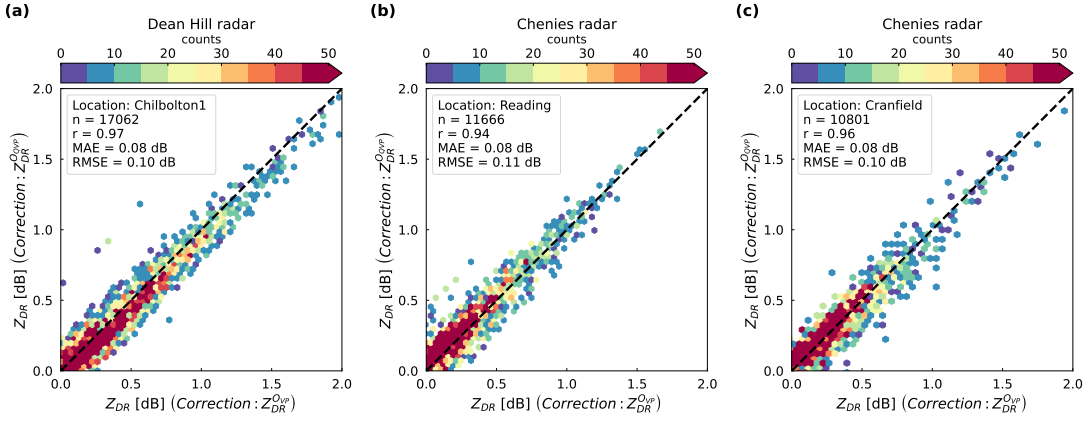

Figure 8. ~~Correlation~~ Scatterplots between ~~two different approaches to correct the~~ calibrated Z_{DR} ~~offset~~measurements using VPs and QVPs. Each ~~scatter density~~ plot represents ~~Z_{DR} measured by the~~ radar Z_{DR} measurements at different locations and filtered using precipitation and intensity classifiers gathered from disdrometers.

Figure 8 shows the scatterplots using both methods ~~used to correct the~~ to calibrate Z_{DR} ~~offset at the~~ measurements at disdrometer locations. For the Chenies radar data, we applied ~~Eq.~~ Equations (7) and (11) to correct the Z_{DR} offset in PPI scans taken at 0.5° elevation angle, whilst for the Dean Hill data, we applied the same equations to correct the Z_{DR} offset but on PPI scans taken at 2° elevation angle as lower elevations are beam-blocked or ~~clutter-contaminated~~contaminated with ground clutter. The proposed approach based on QVPs proves effective as ~~an accuracy~~ accuracy of ~ 0.1 dB is achieved in all analysed cases when comparing the Z_{DR} measurements calibrated using QVPs against Z_{DR} measurements calibrated using the traditional method based on VPs.

In addition, we compare the polarimetric variables measured by the radar with the variables derived from disdrometer DSDs. We discard data not related to liquid precipitation by using the classifiers available on the disdrometer data sets and using only radar data with corresponding values of $\rho_{HV} \geq 0.98$. As described in Section 2.1, algorithms for removing non-meteorological echoes and for correcting the signal attenuation are applied to radar data sets when appropriate. Regarding the disdrometer data sets, we applied a moving average filter (window size = 5) to reduce data fluctuations due to the ~~higher~~ finer time resolution of the disdrometer data ~~than~~ (1-min) compared to the radar data sets (5-min). Furthermore, to include data collected by the CFARR Chilbolton disdrometer (model Joss–Waldvogel, not capable of classifying the rain type), we used the classification from the Thies disdrometer (Chilbolton1) to discard data from the former not related to rain, as these two disdrometers are close to each other (just a few meters apart).

Figure 9 shows the comparison between calibrated Z_{DR} ~~measured by both radars~~ radar measurements and Z_{DR} derived from disdrometer observations ~~located near the radar sites and~~ collected throughout one year of precipitation events. The ~~top row of Figure 9shows calibrated radar~~ Z_{DR} measurements shown in Figures 9(a) were calibrated with VPs whereas the Z_{DR} measurements ~~using the method based on VPs and~~ shown in Figures 9(b) were calibrated with QVPs. The results show comparable errors using either of the Z_{DR} ~~derived from disdrometers. Similarly, Figure 9(b) shows disdrometer and radar~~ calibration methods, confirming the good performance of the proposed method (the MAE and RMSE are below 0.3 dB and 0.4, respectively, in all disdrometer sites for both calibration methods). Although these errors are more significant than the errors shown in Figure 8, these are also due to additional factors such as sampling errors (e.g., comparing point disdrometer observations with areal radar measurements), variations of Z_{DR} measurements ~~. The Z_{DR} radar observations are offset-corrected using the proposed approach based on QVPs.The scatter plots are very similar to those obtained using the~~ aloft (e.g. comparing radar observations aloft with ground disdrometer observations), timing errors (e.g. disdrometer measurements are integrated over time each minute, whereas radar observations are taken in a few seconds every 5-min) and uncertainty in the estimation of Z_{DR} ~~correction method based on VPs, thus reaffirming the good performance of the proposed method~~from DSD measurements. As mentioned above, scans taken at different elevation angles are used on each radar to capture the precipitation occurring above the disdrometer, adding some uncertainty to the interpretation of these results. ~~An in-depth analysis of these results is provided in Section 5.~~

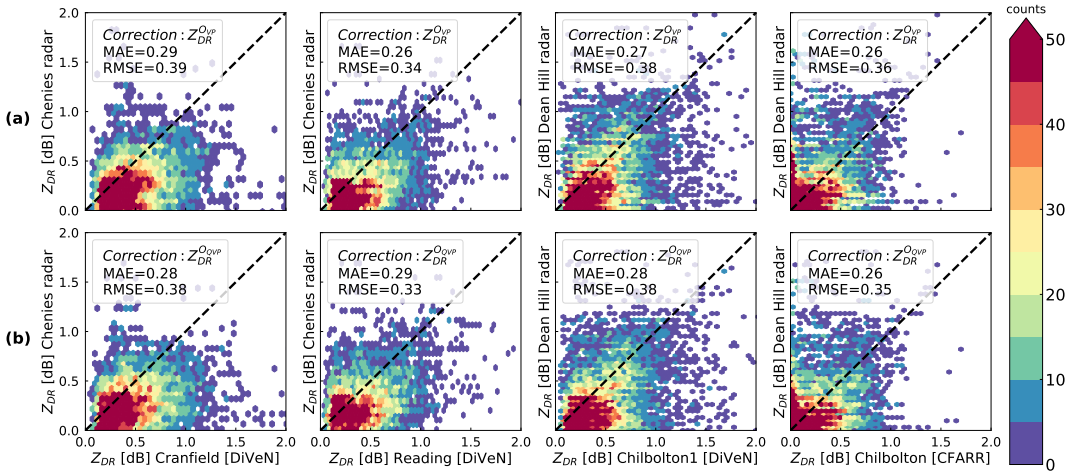

Figure 9. Scatterplots between radar and disdrometer Z_{DR} measurements at several locations: (a) shows scatter density plots of Z_{DR} offset-corrected using VPs at two different radar sites versus Z_{DR} derived from disdrometer data; (b) shows the same as in (a) but the radar Z_{DR} measurements are calibrated applying the QVPs-based method.

4.2.1 Case study: 24 May 2018

Figure 10 portrays a rain event recorded by the Dean Hill radar at an ~~angle elevation~~ elevation angle of 2° and data from ~~the disdrometers described above~~two disdrometers located at the same location (Chilbolton Observatory). The top panel shows a good agreement between the radar reflectivity and the reflectivity derived from disdrometer DSDs as there is a similar trend on all data sets. Overall, the correlation of Z_H for the whole year of data between ~~both radar data sets and several disdrometers is ≥ 0.75 in all the cases~~ the radar data set and the two disdrometers is ≥ 0.80 (graph not shown). On the other hand, the bottom panel of Figure 10 illustrates the ~~radar differential reflectivity offset-corrected by both~~ calibrated Z_{DR} measurements by both methods and the ~~birdbath-scans-based method and using the proposed QVPs-based approach; differential reflectivity derived from DSD data from two nearby disdrometers is also displayed~~Z_{DR} measurements derived from disdrometers observations. It can be seen that the ~~proposed method is~~ Z_{DR} measurements calibrated with the proposed QVP-based method are in good agreement with the ~~'true offset' computed from~~ Z_{DR} measurements calibrated with scans collected at vertical incidence as a maximum difference of ± 0.1 dB is observed. ~~Even more, both~~ Both methods are consistent with the data derived from the two disdrometers ~~. Further discussion of these results is provided in Section 5.~~ located at the Chilbolton Observatory.

4.2.2 Case study: 14 October 2018

Figure 11 shows data collected by the Chenies radar at an elevation angle of 0.5° and data from two disdrometers (Cranfield and Reading) located at different locations. As above, Z_H values are similar on the three devices. Figure 11(a) shows that the radar tends to underestimate the reflectivity, with differences in the order of 5-10 dBZ between the radar data and the Cranfield disdrometer, especially at times between 05:30 am and 08:00 am. For this site, the correlation of Z_H for the whole year of

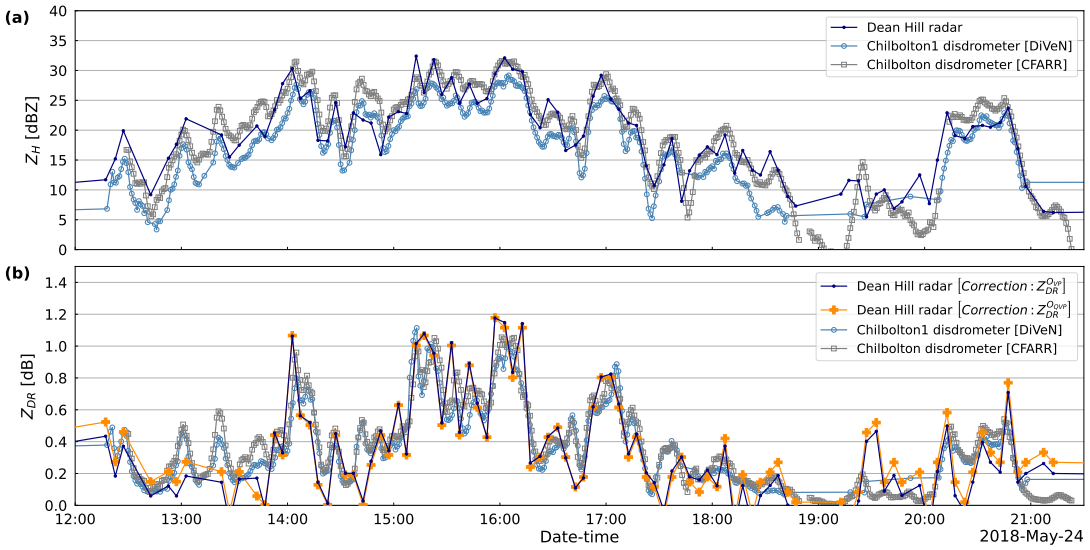

Figure 10. Time-series of disdrometer and radar data related to a precipitation event registered at south England; (a) Reflectivity (Z_H) simulated from disdrometer DSD data at two nearby locations and Z_H measured by the C-band Dean Hill weather radar at an angle elevation of 2°; (b) Differential reflectivity (Z_{DR}) measured by the Dean Hill radar and offset-corrected using two different approaches and Z_{DR} simulated from two disdrometers.

data between the radar data set and the disdrometers is acceptable ($r \approx 0.7$) considering the distance between devices (graph not shown). Consequently, Z_{DR} measured by the radar is in general smaller compared to the Z_{DR} derived from the Cranfield disdrometer (see Figure 11(b)). However, it is important that both Z_{DR} calibration methods yield similar trends on both VPs and QVPs based methods, where maximum differences of 0.2 dB are observed for a short period of time, between 08:30 am and 08:45 am.

On the other hand, Figures 11(c),(d) shows data measured by the Chenies radar and the Reading disdrometer. It can be seen that there is an excellent agreement between devices for both Z_H and Z_{DR}. It is important that Z_{DR} corrected using the proposed method based on QVPs exhibit almost the same pattern compared to the Z_{DR} values corrected using the VP-based method.

5 Discussion

~~We investigate~~ This work reviews the use of ~~quasi-vertical profiles of polarimetric variables~~ QVPs of polarimetric radar measurements to estimate and monitor the overall system bias (or offset) in the differential reflectivity~~Z_{DR}~~. Although several sources of error affect this variable, we focused on detecting and correcting the overall system bias. It is important to ~~keep~~ calibrate Z_{DR} ~~calibrated~~ measurements as this variable is a crucial input to hydrometeor classification methods (Al-Sakka et al., 2013; Park et al., 2009), attenuation corrections schemes (Bringi et al., 2011; Gou et al., 2019) or QPE algorithms (Chan-

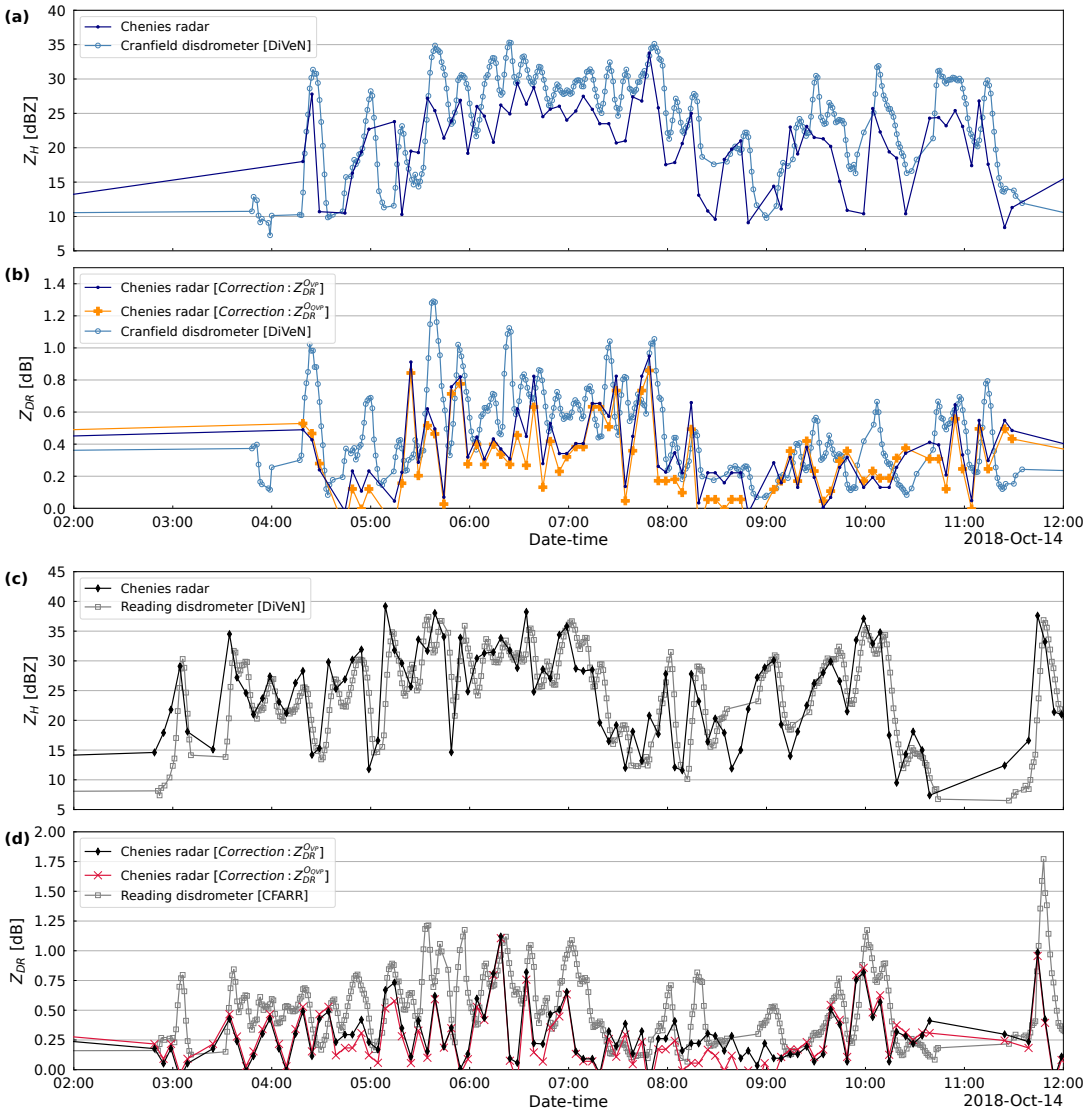

Figure 11. Time-series of disdrometer and radar ~~data related to~~ measurements. a~~precipitation event registered at south England; (a) Reflectivity (Z_H) simulated from disdrometer DSD data at two nearby locations~~ and ~~Z_H measured by a C-band weather radar at an angle elevation of 2; (b~~c) ~~Differential~~ shows the reflectivity ~~(Z_{DR}~~whereas b) ~~measured by the radar~~ and ~~offset-corrected using two different approaches and Z_{DR} simulated from two disdrometers~~d) shows the differential reflectivity.

drasekar and Bringi, 1988; Cifelli et al., 2011; Giangrande and Ryzhkov, 2008; Ryzhkov et al., 2005b; Vulpiani et al., 2009). ~~Previous research has~~ Ryzhkov et al. (2005a) demonstrated that keeping ~~Z_{DR} well-calibrated, i.e., the bias is less than 0.2 dB ,~~ the bias below ± 0.2 dB generates accurate and reliable radar products~~(Ryzhkov et al., 2005a)~~.

~~First, we implemented an operational procedure to detect the offset based on the rationale proposed by Gorgucci et al. (1999) using~~ Previous works have developed methods to compute the Z_{DR} offset using different targets, like light rain (Bechini et al., 2008; Gorguc , dry snow (Ferrone and Berne, 2021; Ryzhkov et al., 2005a), ice (Bringi et al., 2006), sun spikes (Chu et al., 2019; Holleman et al., 2010) or turbulent eddies (Richardson et al., 2017). Most of these methods are based on measurements taken at ~~vertical incidence. The key assumption of this method is that the intrinsic value~~ high elevation angles that reduce the intrinsic variability of Z_{DR}~~in light rain is 0 dB; values deviated from this criterion can be related to the Z_{DR} offset . A similar rationale has been implemented on several radar campaigns confirming its reliability by keeping the~~ . However, mechanical restrictions may prevent some radars from scanning at such high elevation angles; therefore, we evaluate a new approach to compute and correct the offset in radar Z_{DR} ~~offset below 0.1 dB (Bechini et al., 2002; Frech and Hubbert, 2020; Gourley et al., 2009; Louf et al., 2019). We use vertical profiles~~ measurements based on QVPs of polarimetric variables ~~to implement our approach and proposed thresholds to discard data unrelated to light rain. An important condition before applying this approach relies on detecting the melting layer, as this enables the identification of echoes related to liquid precipitation.~~

~~Figures 3 and 4(a) illustrate important aspects of this method. It is important to remark that the VPs represent averaged measurements taken while the radar rotates through 360~~built from PPI scans taken at lower elevation angles of around 9°~~, as depicted in Figure 2(a) . Then, a collection of VPs related to a precipitation event recorded by a C-band weather radar is shown in the left panel of Figure **??**. This plot shows that a major limitation of this approach is when the melting layers are at a relatively low height, and bins related to light rain are not available. Furthermore,~~ . The proposed method is an alternative method to calibrate Z_{DR} measurements, but the traditional method based on VPs should be used instead if these vertical scans are available. As described in Section 3.2, we set light rain as the target to compute the Z_{DR} offset using QVPs mainly to reduce the variability of Z_{DR}. Regarding the selection of this natural target, it is worth saying that we also explored the use of dry snow to derive the Z_{DR} offset. Dry aggregated snow can be found 1 or 2 kilometres above the melting layer in stratiform clouds (Brandes and Ikeda, 2004; Ryzhkov et al., 2005a). Ryzhkov et al. (2005a) explored high elevation angle scans ($\sim 40°$-$60°$) and observed that dry aggregated snow yields distinctive polarimetric signatures, i.e., values of Z_{DR} close to 0 dB, demonstrating that this target can be used to detect the Z_{DR} offset. Consequently, we analysed hundreds of polarimetric profiles (both VPs and QVPs datasets) and found that such signature of dry snow is only observable on the VPs in our data ~~sets, the first kilometre of~~ set. This effect can be seen in Figure 5(a), where similar values of Z_{DR} can be seen on both light rain (below the melting layer bottom) and dry snow (above the melting layer top). Conversely, in the QVP data set (obtained at lower elevation angles of 9°), we observed that values of Z_{DR} in the ~~VPs is contaminated by spurious echoes, thus reducing the number of available bins to implement this method, e. g., at times between 15:00 and 17:00 hours, the melting level bottom (upper boundary of the~~ rain medium ~~) ranges between 1.2-1.3 km; hence only a few bins are available within the VPs to compute the offset. It also notable that Z_{DR} values within and above the melting layer are quite unrelated to the Z_{DR} offset computed from values taken in the rain medium~~were not consistent with those observed aloft, as shown in Figure 5(b). This lack of clear signatures

of dry snow on QVPs is probably related to the beam broadening and non-uniform beam filling effects, expected when the QVPs intercept the ML and regions above at 9°elevations. As shown in the right panel of Figure ??5(b), the standard deviation (blue area) increases within and above the ML due to the presence of mixed-phase particles~~, snow or ice~~; hence complicating the estimation of the Z_{DR} offset using such meteorological targets. This is the reason why we could not use QVPs built from relative low elevation angle scans (<10°) and set dry-snow as the target to derive the Z_{DR} offset.

~~These conditions restrict the implementation of the method based on VPs and, coupled with mechanical restrictions of some weather radars that hamper performing birdbath scans , had lead to developing alternative methods to correct the offset in~~ But using QVPs in light rain events for detecting the Z_{DR} ~~(e. g., see Bechini et al. (2008); Bringi et al. (2006); Chu et al. (2019); Ferrone and B , among others)~~ offset also presents several risks. First, it is important that there is an inherent variability of Z_{DR} in light rain. This is shown in Figure 4(a) where it can be seen that the variability of Z_{DR} increases with larger values of Z_H. Thus, we ~~present a novel approach to detect and correct the offset in the radar~~ propose a constraint to reduce the variability of Z_{DR}~~that can be applied to quasi-vertical profiles of polarimetric variables built from PPI scans taken at elevation angles of around 10.~~

~~As described in Section 3.2, this method is similar to the method based on VPs, but the intrinsic value of~~ , i.e., $0 < Z_H < 20$. This range is a compromise to avoid having significant variations on Z_{DR} ~~in light rain is derived using disdrometer data instead. We limit our method to elevation angles of around 10because using much lower angles to generate QVPs yields vague polarimetric signatures. On the contrary, using greater elevation angles adds uncertainty to the premise described in Eq. (9) and illustrated in Figure 3, where~~ but still keep enough QVPs related to light rain into the analysis and enable the reliable detection of the Z_{DR} ~~measurements much vary when the elevation angles start to increase. It is also important to discuss the imposed~~ offset. In addition, the inherent averaging process in the QVP construction may wash out some key microphysical processes within the precipitation events. Thus, we proposed several constraints to minimise these effects. For example, we imposed a limit of 3 kilometres in height within the QVPs to apply our method: as shown in Figure 2(b), the coverage of the PPI scans at 9° elevation angle captures a mostly uniform volume in the rain region (below 2.5 km). For this elevation angle and a height of 3 km, the base diameter of the cone is around 37 km. Hence we consider that the azimuthal averaging procedure to generate the QVPs below this height reduce deviations in Z_{DR} and enables proper monitoring of the calibration of this variable. Additionally, we define thresholds to discard values within QVPs not related to light rain, e.g., Figure ?? 5(b) shows a collection of QVPs related to a rain event. Most of the QVPs ~~show~~ shows a constant value of Z_{DR} below the ML, whilst outlier values can be discarded by checking their corresponding values on the QVPs of Z_H and ρ_{HV} (plots not showed). This ~~plot~~ figure also shows that the values of Z_{DR} ~~outside~~ above the rain region are loosely correlated to the Z_{DR} offset~~; hence we consider that using~~ , hence hampering the use of meteorological targets like snow or ice~~is not feasible for our method. Finally, we used data derived from three different models of disdrometer and located at different locations to produce robust $Z_H - Z_{DR}$ dependencies that are used to estimate the intrinsic value of Z_{DR} in light rain , as shown in Figure ??. This value is applied in Eq. (10), later used to estimate the offset in the QVPs of Z_{DR}~~. It is clear that dry snow has lower natural Z_{DR} variability compared to light rain when using high tilts (40°-60°). However, this variability increases at lower elevations and the QVPs are affected by this issue. This is why we restricted the height within the QVPs along with thresholds in ρ_{HV} in an effort to keep the variability at the minimum.

~~As mentioned above, there are several methods proposed in the literature to detect and monitor the offset in~~ It is worth mentioning that setting the boundaries of the melting layer correctly within the QVPs is a critical step towards detecting reliable values of the Z_{DR} ~~not based on VPs and making use of other atmospheric targets. But most of them are limited by radar mechanical restriction to point vertically; hence comparing its results with the 'true offset' computed from VPs is not feasible. Even more, none of them uses~~ offset, as this enables the identification of echoes related to liquid precipitation. Allabakash et al. (2019); Griffin et al. (2020); Lukach et al. (2021); Sanchez-Rivas and Rico-Ramirez (2021) demonstrated that heights of the ML top and bottom could be accurately estimated using QVPs. We consider that QVPs without ML signatures are filtered by this requirement, thus reducing the uncertainty of using QVPs of polarimetric variables ~~(a more broadly used tool in recent years) to estimate~~ that do not depict light stratiform rain.

To validate the proposed approach, we implemented an operational procedure to detect the Z_{DR} offset ~~; hence, we carry out a thorough comparison between our proposed method and the method based on birdbath scans.~~

using light rain measurements taken at vertical incidence. This method was proposed initially by Gorgucci et al. (1999), and it is a boilerplate practice that has been tested on several radar campaigns and has confirmed its reliability by keeping the Z_{DR} offset below 0.2 dB (Bechini et al., 2002; Frech and Hubbert, 2020; Gourley et al., 2009; Louf et al., 2019). Figures 6 and 7 show the good agreement between both methods: the proposed method based on QVPs ~~achieves an overall accuracy of around~~ shows maximum differences of 0.1 dB ~~on the calibration of Z_{DR}~~ compared to the method based on VPs. A few data points exhibit larger variation, but this is mainly caused by ~~unclear~~ vague polarimetric signatures of the ML ~~,~~ (no peaks within the polarimetric profiles, especially on those generated from ρ_{HV} measurements), misleading the ML detection algorithm and, thus, the classification of the particles in the liquid phase. The good performance of the method based on QVPs is also confirmed in Figure 8, where we ~~evaluate only~~ evaluated data classified by the disdrometers as related to light to moderate rain rates ~~.~~ ~~These results are in good agreement with the required accuracy of 0.2 dB established by Ryzhkov et al. (2005a) to generate reliable quantitative precipitation estimates using polarimetric weather radar data. The proposed method proves effective on the calibration of~~ and the differences between both Z_{DR} ~~compared to other methods not based on VPs like Ryzhkov et al. (2005a) ($\approx$ 0.2 dB), Giangrande and Ryzhkov (2005) ($\approx$ 0.3 dB), or Bechini et al. (2008) ($\approx$ 0.1 dB), improving the accuracy on the Z_{DR} calibration.~~ calibration methods remain around 0.1 dB

~~Finally, Figures 9and 10 portrays~~ Figures 9-11 show a comparison between radar and disdrometer data. ~~Before analysing these results, it~~ It is important to keep in mind ~~factors~~ that there is some uncertainty in the interpretation of these results, such as (i) the spatial distribution of radar measurements and the well-known discrepancy when comparing it to a fixed point location, (ii) the impact of the signal attenuation in Z_H and Z_{DR}, (iii) the distance between the radars and the disdrometers, (iv) the use of PPI scans collected at higher elevation containing issues related to beam blockage or clutter contamination and (v) the different temporal resolution of each device. ~~It is important to remark that the comparison shown on both plots is made using disdrometer data smoothed using a moving average filter (window size = 5 min) . Regarding~~ However, the errors (MAE and RMSE) between Z_{DR} ~~, the global correlation between the data sets is acceptable ,~~ measured by the radar and Z_{DR} derived from disdrometers are below 0.4 dB in all cases, which is acceptable considering the factors mentioned above but also that this analysis includes one year of data related to precipitation events. Furthermore, we compared the disdrometer derived Z_{DR} ~~with~~

575 ~~the~~ measurements with radar Z_{DR} measurements but without applying the offset correction procedure, and we observed bigger discrepancies between data sets, reaching differences in the order of 1 dB (plots not shown). ~~A higher correlation is observed when comparing data from the Dean Hill radar and the Chilbolton1 disdrometer. This can be explained by the distance between devices (~ 20 km) and the hydrometeor classification available in this disdrometer. The case study shown in Figure 10 confirms~~

580 Finally, the case studies shown in Figures 10 and 11 confirm the good performance of the proposed method to correct the Z_{DR} offset. These events, related to moderate to intense rain events, exhibit differences below ± 0.2 dB. These results are in good agreement with the required accuracy established by Ryzhkov et al. (2005a) to generate reliable quantitative precipitation estimates using polarimetric weather radar data.

6 ~~Summary and Outlook~~Conclusions

585 In this work, we have evaluated different methods for monitoring the calibration of the radar differential reflectivity (Z_{DR}). ~~The most important findings are summarized herein: We implemented a well-known methodology to calibrate and monitor the~~ We explored the use of vertical profiles to calibrate the radar differential reflectivity. Light rain or dry snow are excellent targets to detect the Z_{DR} ~~offset using vertical profiles of polarimetric variables. The method is based on the intrinsic value of Z_{DR} collected in light rain. We~~ offset, and we consider that these methods must be used when possible. However, some radar
590 systems cannot perform scans at such high elevation angles. Thus, we proposed a novel, operational method to calibrate Z_{DR} using ~~quasi-vertical profiles~~ QVPs of polarimetric variables ~~. There are two main advantages of this approach over the method based on VPs: (i) it can be implemented on radars not capable of performing scans~~ built from low elevation scans. This method has the main advantage of not depending on scans taken at vertical incidence ~~,~~ or high elevation angles. However, it relies on detecting QVPs depicting stratiform light rain events (common in the UK), but it may not be suitable for places where heavy
595 rain events are recurrent. Moreover, we are not suggesting that our approach should replace the well-known Z_{DR} calibration method based on birdbath scans.

In addition, we carried out several trials using other meteorological targets like dry snow, but the results were inconclusive. Targeting areas above the melting layer exacerbate the beam broadening and non-uniform beam filling problems as the range increases. These circumstances complicate using dry snow or other solid phase targets to detect the Z_{DR} offset on QVPs built
600 from relative low elevation scans. Thus, we selected the use of light rain, but we proposed several constraints to minimise the variability of Z_{DR} in this media. Future work may implement a previous hydrometeor classification on the QVPs to improve this method. The proposed method is based on a reference Z_{DR} value expected at ground level derived from a wide range of DSDs using a range of parameters expected in real storm events. This value (~~ii)it can detect the offset on rain events not happening exactly above the radar. Although the intrinsic value of~~ 0.18 dB) was computed using constraints related to light rain
605 using Z_H. Additionally, we compared this theoretical Z_{DR} ~~required to implement the method based on QVPs was calculated using disdrometers at different locations and different types and models of disdrometers; this value could be re-calculated~~

~~using disdrometer data near to the radars that want to be calibrated.~~ value to real data derived from disdrometer observations, observing consistency between data.

We applied both methods ~~over one year of~~ to precipitation events collected by two C-band weather radars ~~.~~ for the whole year of 2018. The proposed method to detect the offset in Z_{DR} using QVPs was compared against the ~~'true offset' computed from the~~ "true offset" computed from VPs. We observed ~~an excellent~~ a good agreement between both methods, as the MAE and the RMSE are within ± 0.1 dB. ~~We observed that the~~ However, we are aware that this is a relative evaluation; thus, we also implemented evaluation methods using disdrometer measurements. We compared radar Z_{DR} ~~offset varies daily, or even hourly, hence it is necessary to monitor the calibration of Z_{DR} to generate reliable polarimetric radar products. We compared Z_{DR} measured by the radars~~ measurements with Z_{DR} measurements derived from disdrometer ~~measurements~~observations, obtaining a good agreement between the various data sets. ~~However, it is important to keep in mind that we also applied other procedures like the signal attenuation correction to the radar observations. Even more, the distance between some disdrometers and the radars increases up to 40 km in some cases. These factors add some uncertainty to the interpretation of the results.~~ This long-term evaluation of our method includes different types of precipitation events, ranging from light to heavy rain. We consider that this evaluation process demonstrates the efficacy of the proposed constraints to filter unsuitable QVPs. The proposed method using QVPs generated from PPIs proved to be effective for calibrating and monitoring the radar differential reflectivity ~~. Our results are similar~~ as our results are close to those produced by the traditional method that uses birdbath scans.

Data availability. Disdrometer data collected by the Chilbolton Facility for Atmospheric and Radio Research (CFARR) are available at https://catalogue.ceda.ac.uk/uuid/aac5f8246987ea43a68e3396b530d23e; Chenies C-band rain radar dual polarisation products are available at https://catalogue.ceda.ac.uk/uuid/bb3c55e36b4a4dc8866f0a06be3d475b; Dean Hill C-band rain radar dual polarisation products are available at https://catalogue.ceda.ac.uk/uuid/5b22789f362c43f3b3d1c65bc30c30ee; DiVeN particle diameter and fall velocity measurements are available at http://catalogue.ceda.ac.uk/uuid/001b9640fdb1453aa95a222ba423580e; disdrometer data collected at the UoB are available from the authors upon request.

Author contributions. DSR was responsible for carrying out the experiments, data analysis and writing of the paper. MARR provided supervision of the work and contributed to the writing of the paper.

Competing interests. The authors declare that they have no conflict of interest.

Acknowledgements. This work was carried out using the computational facilities of the Advanced Computing Research Centre, University of Bristol (http://www.bris.ac.uk/acrc/, last access: ~~05 June~~ 05th November 2021)

Financial support. This research has been supported by the Mexican National Council for Science and Technology (CONACyT; grant no. 637289) and the Engineering and Physical Sciences Research Council (EPSRC; grant no. EP/I012222/1).

References

Al-Sakka, H., Boumahmoud, A. A., Fradon, B., Frasier, S. J., and Tabary, P.: A new fuzzy logic hydrometeor classification scheme applied to the french X-, C-, and S-band polarimetric radars, Journal of Applied Meteorology and Climatology, 52, 2328–2344, https://doi.org/10.1175/JAMC-D-12-0236.1, 2013.

Allabakash, S., Lim, S., and Jang, B. J.: Melting layer detection and characterization based on range height indicator-quasi vertical profiles, Remote Sensing, 11, https://doi.org/10.3390/rs11232848, 2019.

Atlas, D., Srivastava, R. C., and Sekhon, R. S.: Doppler radar characteristics of precipitation at vertical incidence, Reviews of Geophysics, 11, 1, https://doi.org/10.1029/RG011i001p00001, 1973.

Bechini, R., Gorgucci, E., Scarchilli, G., and Dietrich, S.: The operational weather radar of Fossalon di Grado (Gorizia, Italy): Accuracy of reflectivity and differential reflectivity measurements, Meteorology and Atmospheric Physics, 79, 275–284, https://doi.org/10.1007/s007030200008, 2002.

Bechini, R., Baldini, L., Cremonini, R., and Gorgucci, E.: Differential reflectivity calibration for operational radars, Journal of Atmospheric and Oceanic Technology, 25, 1542–1555, https://doi.org/10.1175/2008JTECHA1037.1, 2008.

Besic, N., FiguerasVentura, J., Grazioli, J., Gabella, M., Germann, U., and Berne, A.: Hydrometeor classification through statistical clustering of polarimetric radar measurements: A semi-supervised approach, Atmospheric Measurement Techniques, 9, 4425–4445, https://doi.org/10.5194/amt-9-4425-2016, 2016.

Brandes, E. A. and Ikeda, K.: Freezing-level estimation with polarimetric radar, Journal of Applied Meteorology, 43, 1541–1553, https://doi.org/10.1175/JAM2155.1, 2004.

Bringi, V. N. and Chandrasekar, V.: Polarimetric Doppler Weather Radar, Cambridge University Press, Cambridge ; New York, https://doi.org/10.1017/cbo9780511541094, 2001.

Bringi, V. N., Keenan, T. D., and Chandrasekar, V.: Correcting C-band radar reflectivity and differential reflectivity data for rain attenuation: A self-consistent method with constraints, IEEE Transactions on Geoscience and Remote Sensing, 39, 1906–1915, https://doi.org/10.1109/36.951081, 2001.

Bringi, V. N., Chandrasekar, V., Hubbert, J., Gorgucci, E., Randeu, W. L., and Schoenhuber, M.: Raindrop Size Distribution in Different Climatic Regimes from Disdrometer and Dual-Polarized Radar Analysis, Journal of the Atmospheric Sciences, 60, 354–365, https://doi.org/10.1175/1520-0469(2003)060<0354:RSDIDC>2.0.CO;2, 2003.

Bringi, V. N., Thurai, M., Nakagawa, K., Huang, G. J., Kobayashi, T., Adachi, A., Hanado, H., and Sekizawa, S.: Rainfall Estimation from C-Band Polarimetric Radar in Okinawa, Japan: Comparisons with 2D-Video Disdrometer and 400 MHz Wind Profiler, Journal of the Meteorological Society of Japan, 84, 705–724, https://doi.org/10.2151/jmsj.84.705, 2006.

Bringi, V. N., Rico-Ramirez, M. A., and Thurai, M.: Rainfall estimation with an operational polarimetric C-band radar in the United Kingdom: Comparison with a gauge network and error analysis, Journal of Hydrometeorology, 12, 935–954, https://doi.org/10.1175/JHM-D-10-05013.1, 2011.

Chandrasekar, V. and Bringi, V. N.: Error Structure of Multiparameter Radar and Surface Measurements of Rainfall Part I: Differential Reflectivity, Journal of Atmospheric and Oceanic Technology, 5, 783–795, https://doi.org/10.1175/1520-0426(1988)005<0783:ESOMRA>2.0.CO;2, 1988.

Chu, Z., Liu, W., Zhang, G., Kou, L., and Li, N.: Continuous monitoring of differential reflectivity bias for C-band polarimetric radar using online solar echoes in volume scans, Remote Sensing, 11, https://doi.org/10.3390/rs11222714, 2019.

Cifelli, R., Chandrasekar, V., Lim, S., Kennedy, P. C., Wang, Y., and Rutledge, S. A.: A new dual-polarization radar rainfall algorithm: Application in Colorado precipitation events, Journal of Atmospheric and Oceanic Technology, 28, 352–364, https://doi.org/10.1175/2010JTECHA1488.1, 2011.

Darlington, T., Kitchen, M., Sugier, J., and de Rohan-Truba, J.: Automated real-time monitoring of radar sensitivity and antenna pointing accuracy, in: 31st International Conference on Radar Meteorology, pp. 538–541, 2003.

Ferrone, A. and Berne, A.: Dynamic differential reflectivity calibration using vertical profiles in rain and snow, Remote Sensing, 13, 1–24, https://doi.org/10.3390/rs13010008, 2021.

Frech, M. and Hubbert, J.: Monitoring the differential reflectivity and receiver calibration of the German polarimetric weather radar network, Atmospheric Measurement Techniques, 13, 1051–1069, https://doi.org/10.5194/amt-13-1051-2020, 2020.

Giangrande, S. E. and Ryzhkov, A. V.: Calibration of dual-polarization radar in the presence of partial beam blockage, Journal of Atmospheric and Oceanic Technology, 22, 1156–1166, https://doi.org/10.1175/JTECH1766.1, 2005.

Giangrande, S. E. and Ryzhkov, A. V.: Estimation of Rainfall Based on the Results of Polarimetric Echo Classification, Journal of Applied Meteorology and Climatology, 47, 2445–2462, https://doi.org/10.1175/2008JAMC1753.1, 2008.

Gorgucci, E., Scarchilli, G., and Chandrasekar, V.: A procedure to calibrate multiparameter weather radar using properties of the rain medium, IEEE Transactions on Geoscience and Remote Sensing, 37, 269–276, https://doi.org/10.1109/36.739161, 1999.

Gou, Y., Chen, H., and Zheng, J.: An improved self-consistent approach to attenuation correction for C-band polarimetric radar measurements and its impact on quantitative precipitation estimation, Atmospheric Research, 226, 32–48, https://doi.org/10.1016/j.atmosres.2019.03.006, 2019.

Gourley, J. J., Tabary, P., and Parent du Chatelet, J.: Data quality of the Meteo-France C-band polarimetric radar, Journal of Atmospheric and Oceanic Technology, 23, 1340–1356, https://doi.org/10.1175/JTECH1912.1, 2006.

Gourley, J. J., Illingworth, A. J., and Tabary, P.: Absolute calibration of radar reflectivity using redundancy of the polarization observations and implied constraints on drop shapes, Journal of Atmospheric and Oceanic Technology, 26, 689–703, https://doi.org/10.1175/2008JTECHA1152.1, 2009.

Griffin, E. M., Schuur, T. J., and Ryzhkov, A. V.: A polarimetric radar analysis of ice microphysical processes in melting layers of winter storms using s-band quasi-vertical profiles, Journal of Applied Meteorology and Climatology, 59, 751–767, https://doi.org/10.1175/JAMC-D-19-0128.1, 2020.

Gunn, R. and Kinzer, G. D.: The Terminal Velocity of Fall for Water Droplets in Stagnant Air, Journal of Meteorology, 6, 243–248, https://doi.org/10.1175/1520-0469(1949)006<0243:TTVOFF>2.0.CO;2, 1949.

Harrison, D., Norman, K., Darlington, T., Adams, D., Husnoo, N., and Sandford, C.: The evolution of the Met Office radar data quality control and product generation system: RADARNET, 37th Conference on Radar Meteorology, p. 14B.2, https://ams.confex.com/ams/37RADAR/webprogram/Manuscript/Paper275684/RadarnetNextGeneration_AMS_2015.pdf, 2017.

Harrison, D. L., Norman, K., Pierce, C., and Gaussiat, N.: Radar products for hydrological applications in the UK, Proceedings of the Institution of Civil Engineers - Water Management, 165, 89–103, https://doi.org/10.1680/wama.2012.165.2.89, 2012.

Holleman, I., Huuskonen, A., Gill, R., and Tabary, P.: Operational monitoring of radar differential reflectivity using the sun, Journal of Atmospheric and Oceanic Technology, 27, 881–887, https://doi.org/10.1175/2010JTECHA1381.1, 2010.

Huuskonen, A. and Holleman, I.: Determining weather radar antenna pointing using signals detected from the sun at low antenna elevations, Journal of Atmospheric and Oceanic Technology, 24, 476–483, https://doi.org/10.1175/JTECH1978.1, 2007.

Huuskonen, A., Kurri, M., and Holleman, I.: Improved analysis of solar signals for differential reflectivity monitoring, Atmospheric Measurement Techniques, 9, 3183–3192, https://doi.org/10.5194/amt-9-3183-2016, 2016.

Ji, Chen, Li, Chen, Xiao, Chen, and Zhang: Raindrop Size Distributions and Rain Characteristics Observed by a PARSIVEL Disdrometer in Beijing, Northern China, Remote Sensing, 11, 1479, https://doi.org/10.3390/rs11121479, 2019.

Kumjian, M. R., Mishra, S., Giangrande, S. E., Toto, T., Ryzhkov, A. V., and Bansemer, A.: Polarimetric radar and aircraft observations of saggy bright bands during MC3E, Journal of Geophysical Research, 121, 3584–3607, https://doi.org/10.1002/2015JD024446, 2016.

Louf, V., Protat, A., Warren, R. A., Collis, S. M., Wolff, D. B., Raunyiar, S., Jakob, C., and Petersen, W. A.: An integrated approach to weather radar calibration and monitoring using ground clutter and satellite comparisons, Journal of Atmospheric and Oceanic Technology, 36, 17–39, https://doi.org/10.1175/JTECH-D-18-0007.1, 2019.

Lukach, M., Dufton, D., Crosier, J., Hampton, J. M., Bennett, L., and Neely III, R. R.: Hydrometeor classification of quasi-vertical profiles of polarimetric radar measurements using a top-down iterative hierarchical clustering method, Atmospheric Measurement Techniques, 14, 1075–1098, https://doi.org/10.5194/amt-14-1075-2021, 2021.

Met Office: Chenies C-band rain radar dual polar products. NCAS British Atmospheric Data Centre, https://catalogue.ceda.ac.uk/uuid/bb3c55e36b4a4dc8866f0a06be3d475b, 2013.

Met Office: Deanhill C-band rain radar dual polar products. NERC EDS Centre for Environmental Data Analysis, https://catalogue.ceda.ac.uk/uuid/5b22789f362c43f3b3d1c65bc30c30ee, 2021.

Mishchenko, M. I.: Calculation of the amplitude matrix for a nonspherical particle in a fixed orientation, Applied Optics, 39, 1026, https://doi.org/10.1364/ao.39.001026, 2000.

Natural Environment Research Council, Met Office, Pickering, B., Neely III, R., and Harrison, D.: The Disdrometer Verification Network (DiVeN): particle diameter and fall velocity measurements from a network of Thies Laser Precipitation Monitors around the UK (2017-2019). Centre for Environmental Data Analysis, 31 October 2019, http://dx.doi.org/10.5285/602f11d9a2034dae9d0a7356f9aeaf45, 2019.

OTT HydroMet: Operating instructions Present Weather Sensor OTT Parsivel 2, Tech. rep., GmbH, Kempten, Germany, 2016.

Park, H. S., Ryzhkov, A. V., Zrnić, D. S., and Kim, K. E.: The hydrometeor classification algorithm for the polarimetric WSR-88D: Description and application to an MCS, Weather and Forecasting, 24, 730–748, https://doi.org/10.1175/2008WAF2222205.1, 2009.

Pickering, B. S., Neely III, R. R., and Harrison, D.: The Disdrometer Verification Network (DiVeN): a UK network of laser precipitation instruments, Atmospheric Measurement Techniques, 12, 5845–5861, https://doi.org/10.5194/amt-12-5845-2019, 2019.

Pruppacher, H. R. and Beard, K. V.: A wind tunnel investigation of the internal circulation and shape of water drops falling at terminal velocity in air, Quarterly Journal of the Royal Meteorological Society, 96, 247–256, https://doi.org/10.1002/qj.49709640807, 1970.

Richardson, L. M., Zitte, W. D., Lee, R. R., Melnikov, V. M., Ice, R. L., and Cunningham, J. G.: Bragg scatter detection by the WSR-88D. Part II: Assessment of ZDR bias estimation, Journal of Atmospheric and Oceanic Technology, 34, 479–493, https://doi.org/10.1175/JTECH-D-16-0031.1, 2017.

Rico-Ramirez, M. A.: Adaptive attenuation correction techniques for C-band polarimetric weather radars, IEEE Transactions on Geoscience and Remote Sensing, 50, 5061–5071, https://doi.org/10.1109/TGRS.2012.2195228, 2012.

Rico-Ramirez, M. A. and Cluckie, I. D.: Classification of ground clutter and anomalous propagation using dual-polarization weather radar, IEEE Transactions on Geoscience and Remote Sensing, 46, 1892–1904, https://doi.org/10.1109/TGRS.2008.916979, 2008.

Ryzhkov, A. V., Giangrande, S. E., Melnikov, V. M., and Schuur, T. J.: Calibration issues of dual-polarization radar measurements, Journal of Atmospheric and Oceanic Technology, 22, 1138–1155, https://doi.org/10.1175/JTECH1772.1, 2005a.

Ryzhkov, A. V., Giangrande, S. E., and Schuur, T. J.: Rainfall estimation with a polarimetric prototype of WSR-88D, Journal of Applied Meteorology, 44, 502–515, https://doi.org/10.1175/JAM2213.1, 2005b.

Ryzhkov, A. V., Zhang, P., Reeves, H., Kumjian, M., Tschallener, T., Trömel, S., and Simmer, C.: Quasi-vertical profiles-A new way to look at polarimetric radar data, Journal of Atmospheric and Oceanic Technology, 33, 551–562, https://doi.org/10.1175/JTECH-D-15-0020.1, 2016.

Sanchez-Rivas, D. and Rico-Ramirez, M. A.: Detection of the melting level with polarimetric weather radar, Atmospheric Measurement Techniques, 14, 2873–2890, https://doi.org/10.5194/amt-14-2873-2021, 2021.

Science and Technology Facilities Council, Chilbolton Facility for Atmospheric and Radio Research; Natural Environment Research Council, and Wrench, C.: Chilbolton Facility for Atmospheric and Radio Research (CFARR) Disdrometer Data, Chilbolton Site. NCAS British Atmospheric Data Centre, https://catalogue.ceda.ac.uk/uuid/aac5f8246987ea43a68e3396b530d23e, 2003.

Seliga, T. A. and Bringi, V. N.: Potential Use of Radar Differential Reflectivity Measurements at Orthogonal Polarizations for Measuring Precipitation, Journal of Applied Meteorology, 15, 69–76, https://doi.org/10.1175/1520-0450(1976)015<0069:PUORDR>2.0.CO;2, 1976.

Straka, J. M., Zrnić, D. S., and Ryzhkov, A. V.: Bulk Hydrometeor Classification and Quantification Using Polarimetric Radar Data: Synthesis of Relations, Journal of Applied Meteorology, 39, 1341–1372, https://doi.org/10.1175/1520-0450(2000)039<1341:BHCAQU>2.0.CO;2, 2000.

Thurai, M., Huang, G. J., Bringi, V. N., Randeu, W. L., and Schönhuber, M.: Drop Shapes, Model Comparisons, and Calculations of Polarimetric Radar Parameters in Rain, Journal of Atmospheric and Oceanic Technology, 24, 1019–1032, https://doi.org/10.1175/JTECH2051.1, 2007.

Vulpiani, G., Giangrande, S., and Marzano, F. S.: Rainfall Estimation from Polarimetric S-Band Radar Measurements: Validation of a Neural Network Approach, Journal of Applied Meteorology and Climatology, 48, 2022–2036, https://doi.org/10.1175/2009JAMC2172.1, 2009.

Zrnić, D., Doviak, R., Zhang, G., and Ryzhkov, A.: Bias in differential reflectivity due to cross coupling through the radiation patterns of polarimetric weather radars, Journal of Atmospheric and Oceanic Technology, 27, 1624–1637, https://doi.org/10.1175/2010JTECHA1350.1, 2010.

Zrnic, D. S., Melnikov, V. M., and Carter, J. K.: Calibrating Differential Reflectivity on the WSR-88D, Journal of Atmospheric and Oceanic Technology, 23, 944–951, https://doi.org/10.1175/JTECH1893.1, 2006.